Development/Plasticity/Repair

Lrrn1 Regulates Medial Boundary Formation in the Developing Mouse Organ of Corti

Helen R. Maunsell, Kathryn Ellis, Matthew W. Kelley, and Elizabeth Carroll Driver
Porter Neuroscience Research Center, Laboratory of Cochlear Development, National Institute on Deafness and Other Communication Disorders, Bethesda, Maryland 20892

One of the most striking aspects of the sensory epithelium of the mammalian cochlea, the organ of Corti (OC), is the presence of precise boundaries between sensory and nonsensory cells at its medial and lateral edges. A particular example of this precision is the single row of inner hair cells (IHCs) and associated supporting cells along the medial (neural) boundary. Despite the regularity of this boundary, the developmental processes and genetic factors that contribute to its specification are poorly understood. In this study we demonstrate that *Leucine Rich Repeat Neuronal 1* (*Lrrn1*), which codes for a single-pass, transmembrane protein, is expressed before the development of the mouse organ of Corti in the row of cells that will form its medial border. Deletion of *Lrrn1* in mice of mixed sex leads to disruptions in boundary formation that manifest as ectopic inner hair cells and supporting cells. Genetic and pharmacological manipulations demonstrate that *Lrrn1* interacts with the Notch signaling pathway and strongly suggest that Lrrn1 normally acts to enhance Notch signaling across the medial boundary. This interaction is required to promote formation of the row of inner hair cells and suppress the conversion of adjacent nonsensory cells into hair cells and supporting cells. These results identify Lrrn1 as an important regulator of boundary formation and cellular patterning during development of the organ of Corti.

Key words: **cochlea; development; inner ear; LRRN1; Notch; organ of Corti**

Significance Statement

Patterning of the developing mammalian cochlea into distinct sensory and nonsensory regions and the specification of multiple different cell fates within those regions are critical for proper auditory function. Here, we report that the transmembrane protein Leucine Rich Repeat Neuronal 1 (LRRN1) is expressed along the sharp medial boundary between the single row of mechanosensory inner hair cells (IHCs) and adjacent nonsensory cells. Formation of this boundary is mediated in part by Notch signaling, and loss of *Lrrn1* leads to disruptions in boundary formation similar to those caused by a reduction in Notch activity, suggesting that LRRN1 likely acts to enhance Notch signaling. Greater understanding of sensory/nonsensory cell fate decisions in the cochlea will help inform the development of regenerative strategies aimed at restoring auditory function.

Introduction

Development of the mammalian auditory sensory epithelium, the organ of Corti (OC), requires the interplay of several conserved signaling pathways. For instance, the Hedgehog, Notch, Wnt, Fgf, and Bmp signaling pathways coordinate to partition the early cochlear epithelium into prosensory and nonsensory regions (Groves and Fekete, 2012; Wu and Kelley, 2012). Subsequent signaling events further specify prosensory cells to develop as distinct types of hair cells and supporting cells while nonsensory cells also assume multiple fates (Lanford et al., 1999; Mueller et al., 2002; Ohyama et al., 2010; Jacques et al., 2012). A key step in the initiation of the development of the OC is the onset of differentiation of the single row of inner hair cells (IHCs), located at what will become the medial edge of the OC (Rubel, 1978). The first IHCs appear in the mid-basal region of the cochlear duct, with additional IHCs forming in a contiguous line extending toward the apex. Soon after the formation of the first IHCs, three rows of outer hair cells (OHCs) begin to form

Received Nov. 17, 2022; revised May 12, 2023; accepted June 10, 2023.

Author contributions: H.R.M., K.E., M.W.K., and E.C.D. designed research; H.R.M., K.E., and E.C.D. performed research; H.R.M., K.E., M.W.K., and E.C.D. analyzed data; H.R.M. wrote the first draft of the paper; H.R.M., M.W.K., and E.C.D. edited the paper; H.R.M., M.W.K., and E.C.D. wrote the paper.

This work was supported by the National Institute on Deafness and Other Communication Disorders Division of Intramural Research Grant DC000059 (to M.W.K.). We thank the staff in the Porter Neuroscience Shared Animal Facility for outstanding animal care and Dr. Weise Chang for technical assistance. We also thank Dr. Basile Tarchini and Dr. Doris Wu for reading an earlier version of this manuscript and the staff at the Frederick Transgenic Mouse Model Laboratory for assistance in the generation of *Lrrn1* mutant mice.

H. R. Maunsell's present address: Program in Development, Disease Models and Therapeutics, Baylor College of Medicine, Houston, Texas 77030.

K. Ellis's present address: Decibel Therapeutics, Boston, Massachusetts 02215.

The authors declare no competing financial interests.

Correspondence should be addressed to Elizabeth Carroll Driver at drivere@nidcd.nih.gov or Matthew W. Kelley at kelleymt@nidcd.nih.gov.

https://doi.org/10.1523/JNEUROSCI.2141-22.2023

laterally (Driver and Kelley, 2020). As is the case for IHCs, OHC development also occurs in a wave that extends from base to apex. While developing OHCs undergo considerable migration and rearrangement (Yamamoto et al., 2009; Driver et al., 2017; Cohen et al., 2020), IHCs initially appear within a few cell diameters of their mature position (McKenzie et al., 2004), suggesting that the medial edge, and therefore the medial-lateral axis, of the OC is defined before the onset of IHC development.

IHCs in the mature OC are arranged in a single row, indicating a precise boundary between sensory and nonsensory regions of the duct, but recent work has demonstrated that the formation and maintenance of this boundary is a dynamic process (Basch et al., 2016). In particular, Notch-mediated interactions play a key role in preventing nonsensory cells located adjacent to the medial boundary from assuming a sensory fate (Kiernan et al., 2001, 2006; Basch et al., 2016). Our understanding of how this process occurs, and the genetic factors that regulate it, remains very limited.

In the *Drosophila* wing imaginal disk, Notch interacts with two other transmembrane proteins, Tartan and Capricious, to define and maintain a dorsal-ventral boundary (Blair, 2001; Milán et al., 2001, 2005). Similarly, in vertebrates, an ortholog of Tartan and Capricious, *Leucine Rich Repeat Neuronal 1* (*Lrrn1*), has been implicated as a mediator of rhombomere boundary formation (Andreae et al., 2007), and shown to be involved in specifying the chick thalamus-prethalamus and midbrain-hindbrain boundaries (Tossell et al., 2011). In this study, we demonstrate that *Lrrn1* is expressed along the medial boundary of the OC before hair cell formation and that deletion of *Lrrn1* leads to defects in medial boundary formation. Further, we show that during cochlear development Lrrn1 interacts with the Notch signaling pathway and that Lrrn1 expression is linked to the specification of medial boundary identity. These results demonstrate a key role for Lrrn1 during cochlear medial boundary formation.

Materials and Methods

Animal care

All animals were maintained in the Porter Neuroscience Shared Animal Facility according to the animal care and use guidelines provided by the National Institute of Neurological Disorders and Stroke/National Institute on Deafness and Other Communication Disorders Animal Care and Use Committee of the National Institutes of Health.

Multiplex single molecule fluorescence in situ *hybridization (smFISH)*

For multiplex smFISH on tissue sections, inner ears were dissected from embryonic day (E)14, E16, and postnatal day (P)0 embryos, fixed in 4% paraformaldehyde (PFA) in PBS overnight (O/N) at 4°C, then cryoprotected in sucrose, embedded in OCT, and frozen for cryosectioning. Sections were cut at a thickness of 10 µm. Following sectioning, samples were pretreated and assayed for the fluorescent hybridization following the ACD RNAscope Fluorescent Multiplex Reagent kit protocol (320850; Kolla et al., 2020). Sections were counter-stained with DAPI to visualize nuclei. For whole mount smFISH, cochlea were dissected from E15 embryos, fixed overnight, and processed following the protocol of Kersigo et al., 2018. The following probes were obtained from Advanced Cell Diagnostics: *Pvalb*, *Sox2*, *Lrrn1*, *Hes1*, *Mfng*, and *Lfng*.

Immunostaining

Cochlear whole-mounts and cryosections were incubated in primary antibodies overnight at 4°C. Sheep anti-human/mouse LRRN1 (R&D Systems AF4990, RRID: AB_2234807) was used at 0.1 µg/ml. Other primary antibodies used were rabbit anti-CDKN1B (Thermo Fisher Scientific PA5-16717, RRID:AB_10977242), rabbit anti-MYOSIN6 (Proteus Biosciences 25-6791, RRID:AB_10013626), rat anti-CDH1 (Santa Cruz Biotechnology sc-59778, RRID:AB_781738), rabbit anti-NPY (Sigma-Aldrich N9528, RRID:AB_260814), rabbit anti-FABP7 (Thermo Fisher Scientific PA5-24949, RRID:AB_2542449), rabbit anti-MYOSIN7A (Proteus Biosciences, 25-6790, RRID:AB_10015251), goat anti-FABP7 (R&D Systems, RRID: AB_2100475), goat anti-NGFR (R&D Systems, RRID:AB_2152638), goat anti-PROX1 (R&D Systems AF2727, RRID:AB_2170716), sheep anti-DLL1 (R&D Systems; RRID:AB_2092830), mouse anti-POU4F3 (Santa Cruz Biotechnology sc-81980, RRID:AB_2167543), goat anti-SOX2 (R&D Systems, RRID:AB_355110), rabbit anti-DsRed (Takara Bio 632496, RRID:AB_10013483), mouse anti-Ki67 (Santa Cruz Biotechnology sc-23 900, RRID:AB_627859), and goat anti-JAGGED1 (R&D Systems, AF599, RRID:AB_2128257). All primary antibodies other than anti-LRRN1 were used at 0.4–1 µg/ml. Alexa Fluor-labeled secondary antibodies (0.5 µg/ml) were used in parallel with Alexa Fluor-conjugated phalloidin to label F-actin (1 U/ml); all were obtained from Thermo Fisher Scientific.

Generation of Lrrn1-CreERT2 reporter line and fate mapping of Lrrn1^{+} *cells*

Recombineering was used to replace the coding sequence of Exon 2 of the mouse *Lrrn1* gene (NCBI Gene 16 979, MGI 106038, Ensembl: ENSMUSG00000034648), with a CreERT2-Neo cassette in BAC clone RP24-27107. Transgenic mice were generated through pronuclear injection and incorporation of the transgene was confirmed by PCR. The *Lrrn1-CreERT2* line was then crossed with homozygous *Gt(ROSA)26Sor*$^{tm14(CAG-tdTomato)Hze}$ mice (*Rosa26*$^{tdTomato(tdT)}$; The Jackson Laboratory, strain #007914) to generate *Lrrn1*$^{CreERT2/+}$; *Rosa26*$^{tdT/+}$ transgenic animals. *Lrrn1-CreERT2; Rosa2*$^{tdT/+}$ males were crossed with CD1 wild-type (WT) females, with pregnancies timed based on the appearance of a plug on day embryonic day (E)0. At E12 or E16, 400 µg of tamoxifen (Sigma-Aldrich T5648) was dissolved with 20 mg/ml progesterone (Sigma-Aldrich P0130) in a flax seed oil solution and administered to pregnant females by oral gavage. Pregnancies were maintained until litters were delivered. Pups were euthanized at P0, and inner ears were dissected, fixed, and prepared for immunostaining and analysis.

Cochlear explants

For cell fate analysis, *Lrrn1-CreERT2; Rosa26*$^{tdT/+}$ cochleae were dissected from E14 embryos and established as explants as previously described (Driver and Kelley, 2010). To induce recombination, 4-OH tamoxifen (Sigma-Aldrich 579002) was added at 100 nM or 1 μM for 24 h beginning at immediately at E14 or after 1 d *in vitro* (DIV; E15 equivalent). Explants were maintained for 5 DIV total (P0 equivalent), then fixed and processed for immunostaining.

For *in vitro* inhibition of γ-secretase, cochlear explants were established from *Lrrn1*$^{+/+}$, *Lrrn1*$^{+/-}$, and *Lrrn1*$^{-/-}$ embryos at E14 and treated with media containing 500 pM LY411575 (Sigma SML0506) or control media (0.2% DMSO) for the initial 2 DIV. After 2 DIV, the LY411575-containing media was removed and replaced with control media. Explants were fixed after an additional 3 DIV (P0 equivalent) and processed as described above.

For inhibition of GSK3 activity to disrupt medial-lateral boundary formation, explants were established from CD1 embryonic cochleae at E13 and cultured for 2 DIV, either in control media (0.2% DMSO) or in media containing 2 μM CHIR99021 (Tocris 4423). After 2 DIV, explants were fixed and processed for immunostaining.

Generation of Lrrn1*-TALEN mutant mice*

Five TALENs were designed to target the single coding exon of *Lrrn1* using TALEN targeter and assembled using golden gate cloning. Golden Gate TALEN and TAL Effector kit 2.0 was purchased from Addgene (#1000000024). TALEN gene editing efficiency was tested in Neuro2A cells by GeneCopoeia as follows: Neuro2A cells were transfected with plasmids containing the left and right TALEN arms at a concentration of 0.5 µg each. Cells were collected 48 h post-transfection, genomic DNA was extracted, and an 800-bp region around the TALEN target site was PCR amplified. DNA was melted, slowly re-hybridized and digested with T7 Endonuclease I (NEB catalog #M0302S) to detect mismatched base pairs. One chromosome-level validated TALEN pair was prepared for pronuclear injection into mouse embryos as follows: mRNA was generated from TALEN plasmid using SP6 mMessage mMachine kit

(Thermo Fisher Scientific catalog #AM1340). mRNA was poly-adenylated using Poly(A) Tailing kit (Thermo Fisher Scientific catalog #AM1350). Poly-adenylated mRNA was cleaned using RNeasy Mini clean up kit (QIAGEN catalog #74104). Pronuclear injection of mouse embryos was performed at the Transgenic Mouse Model Laboratory at Frederick National Laboratory for Cancer Research by Leidos Biomedical Research TALEN founders were identified using genomic DNA from mouse tail snips using the T7 Endonuclease I assay as described above, and three independent mouse lines carrying 2-, 4-, or 31-bp deletions in the 10th leucine-rich repeat in the extracellular domain of *Lrrn1*. Each mutation was predicted to result in a frameshift leading to an early stop codon. For all three alleles, no significant changes in cochlear morphology or length were observed in heterozygotes, and homozygous mutants all displayed increased numbers of extra IHC and IPhCs (doublets) medial to the sensory/nonsensory boundary. The 2-bp deletion allele was maintained on a CD1 background, and the 4- and 31-bp alleles were maintained on a C57BL/6J background.

Generation of Lrrn1$^{-/-}$; Notch1$^{+/-}$ *mutant mice*

Male mice carrying a conditional *Notch1* allele (Radtke et al., 1999) were crossed to *Zp3*^{Cre} (de Vries et al., 2000, RRID:IMSR_JAX:003651) females to generate a germline deletion of *Notch1*, then crossed to mice carrying the 2-bp deletion allele of *Lrrn1*. *Lrrn1*$^{+/-}$; *Notch1*$^{+/-}$ mice were crossed to generate *Lrrn1*$^{+/+}$; *Notch1*$^{+/-}$, *Lrrn1*$^{+/-}$; *Notch1*$^{+/-}$, and *Lrrn1*$^{-/-}$; *Notch1*$^{+/-}$ animals. These mice were maintained on a mixed background including the outbred CD1 strain.

Cochlear imaging and cell counts

All imaging of cochlear whole-mounts, sections, and explants was performed on a Zeiss LSM710 or LSM900 confocal microscope. Images shown are XY Z-stack projections or orthogonal YZ views, as indicated.

The number of ectopic IHCs and IPhCs per unit length was determined by measuring the total length (μm) of each cochlea, dividing each cochlea into thirds, designated as apical, middle, and basal regions, and then counting the number of ectopic IHCs (MYO7A+) and IPhCs (FABP7+) that appeared next to the single row of IHCs aligned adjacent to the pillar cells and IPhCs along a cochlear length of 1000 μm (~1/3 of the cochlear length).

To quantify the density of IHCs in γ-secretase inhibitor-treated explants, the total length of each explant was measured. The apical-most 25% of each explant was excluded from analysis because of the high morphologic variability in this region in explants. All IHCs (MYO7A+ cells medial to the pillar cell region) were counted in the basal 75% of each explant, divided by the length of that portion of the explant in μm, and shown as that value per 100 μm.

Comparisons of the intensity of *Hes1* expression detected by smFISH were made from images taken 250 μm from the base of E15 *Lrrn1*$^{+/+}$ or *Lrrn1*$^{-/-}$ cochleae. All images were obtained with identical LSM acquisition settings. We generated Z-stack projection images with a depth of 1.5 μm (from five optical slices), starting 1.5 μm from the luminal surface of the HCs. Using ImageJ, we measured the average *Hes1* pixel intensity in 40 × 8 μm rectangular regions of interest (ROIs) at equivalent base-to-apex positions, both lateral to the third row of OHCs and medial to the IHCs. The ratio of the average intensity of *Hes1* expression in the medial ROI to the lateral ROI was calculated.

Graphs and statistical analyses

Graphs were created in GraphPad Prism. Cell counts and measurements are shown as box and whisker plots, with the box extending from the 25th to 75th percentile, whiskers to the minimum and maximum values, and a line indicating the median. For *Lrrn1*$^{-/-}$ phenotype analysis, we collected and compared cochleae from eight *Lrrn1* mutants with the 4-bp deletion to eight heterozygous littermates, pooled from three different litters for biological replicates. Two 31-bp deletion *Lrrn1* mutants and one heterozygous littermate were also included in the analysis. Extra IPhCs were counted in four mutant and four heterozygous *Lrrn1* samples from two litters. Analysis of the mutant and heterozygous genotypes was performed by independent, two-tailed, unequal variance Student's *t* tests, which specifically compared counts of the respective cell type per cochlear region [e.g., ectopic IHCs/(1/3 cochlear length)] to give the estimated number of that cell type per 1 mm in the apex, middle, and base of each sample. Significance annotated by ** ($p \leq 0.01$), *** ($p \leq 0.001$), and *** ($p \leq 0.0001$). A Holm–Šidák test was used to correct for multiple comparisons per analysis.

For lineage tracing analysis in *Lrrn1-CreERT2*; *Rosa26*^{tdTomato} mice, in vivo cell labeling was sparse, so we performed our quantification with respect to all of the cells labeled per time point (E12 or E16). Following characterization and quantification of the distinct cell types labeled in the cochlear sensory epithelium, we then calculated the proportion of each type relative to the total labeled. For multiple comparisons, a two-way ANOVA was performed, comparing the effect of both the stage of Cre induction (E12 and E16) and the specific cell types labeled (IHC, IPhC, Border, Deiters, Pillar). This was followed by Tukey's multiple comparison test. Statistically significant differences between genotypes or treatments were determined using Welch's *t*-test.

A mixed-model (Type III) two-way ANOVA and Tukey's test were similarly used to assess the effect of Lrrn1 and Notch1 genotypes and their potential interaction on the number of extra IHCs, endogenous IHCs (Fig. 6*B*,*C*) and OHCs (data not shown); *p*-values were adjusted for multiple comparisons according to the Holm–Šidák method. To quantify the changes in cell shape and density observed in *Lrrn1*$^{-/-}$; *Notch1*$^{+/-}$ cochleae ($N = 54$ cells, 7 cochleae) relative to *Lrrn1*$^{-/-}$; *Notch1*$^{+/+}$ cochleae ($N = 76$ cells, 7 cochleae), we analyzed high magnification images of the middle regions of each sample. Data on parameters including the area and perimeter of individual, intact cells in each image were collected using the Analyze Particles and Measure tools in ImageJ.

Differences in the density of total IHCs in LY411575-treated explants compared with control explants were determined by ordinary one-way ANOVA, followed by Šidák's multiple comparisons test. Differences in the ratios of medial to lateral *Hes1* expression were determined by unpaired, two-tailed *t* test.

Results

Lrrn1 is expressed in cells at the medial boundary of the embryonic and neonatal OC

Analysis of single-cell RNAseq data from the developing cochlear duct indicated that *Lrrn1* expression is predominantly, but not exclusively, expressed in cells located at the medial boundary of the OC at embryonic day (E)14, E16, and postnatal day (P)1 (Fig. 1*A*,*B*; data not shown). To determine the timing of onset and localization of *Lrrn1* during cochlear development, we performed single molecule fluorescence *in situ* hybridization (smFISH) on inner ear sections from E14, E16, and P0. E14 sections were also hybridized with a probe against *Sox2*, which marks the prosensory domain (Kiernan et al., 2005). In the cochlear base at E14, *Lrrn1* mRNA is expressed in a narrow band, possibly only the width of a single cell, that overlaps with expression of *Sox2* near the medial edge of the prosensory domain (Fig. 1*C*).

At E16, *Parvalbumin* (*Pvalb*) is expressed in developing IHCs located in the basal and middle turns of the cochlea (Xiang et al., 1998), and can be used to locate the medial boundary. In sections that are double labeled for *Pvalb* and *Lrrn1*, the two markers strongly overlap (Fig. 1*D*), confirming localization of *Lrrn1* to the medial edge of the prosensory domain. Finally, in sections of P0 cochleae, *Lrrn1* expression continues to overlap partially with *Pvalb* in cells along the medial edge of the OC (Fig. 1*E*). However, the intracellular pattern of *Lrrn1* expression does not fully overlap with *Pvalb* (Fig. 1*E*"), suggesting that *Lrrn1* may be expressed in cells other than hair cells, most likely inner phalangeal cells (IPhCs), based on location. These results indicate that *Lrrn1*

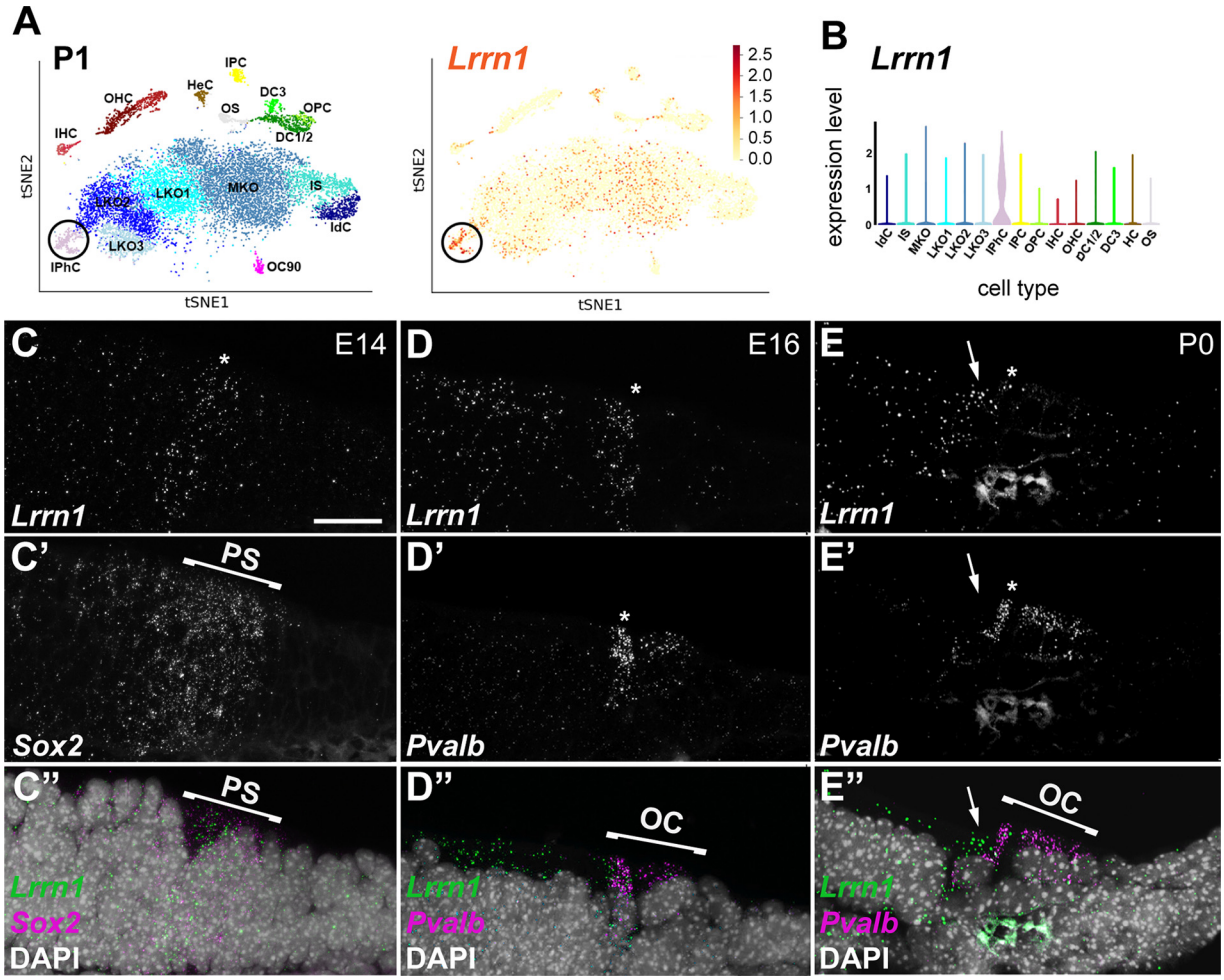

Figure 1. Expression of *Lrrn1* is restricted to the medial edge of the developing OC. ***A***, t-distributed Stochastic Neighbor Embedding (tSNE) plot of P1 cochlear single cells based on single-cell RNAseq results generated using the gEAR website (Orvis et al., 2021). Left side image depicts different cell types as labeled. Circle indicates inner phalangeal cells (IPhC). Right side image shows expression of *Lrrn1* in the same plot. Note increased expression in the IPhC group (circle). ***B***, Violin plot for expression of *Lrrn1* in the same data as in ***A*** generated using gEAR. Note that only IPhCs show consistent increased expression of *Lrrn1*. ***C–E***, Confocal images of smFISH sections through the basal turn of the cochlea from WT mice at E14, E16, and P0. ***C***, ***C'***, At E14, expression of *Lrrn1* overlaps with *Sox2*, a marker of the prosensory domain (asterisk, bracket). In ***C''***, the bracket indicates the prosensory domain (PS) and cell nuclei are labeled with DAPI. ***D***, At E16, expression of *Lrrn1* overlaps with *Pvalb*, a marker of developing IHCs (asterisk). The bracket in ***D''*** indicates the developing organ of Corti (OC). ***E***, At P0, *Lrrn1* is still co-localized with *Pvalb* but the intracellular labeling pattern appears different, likely indicating *Lrrn1* expression in IPhCs at this stage (arrows). Scale bar in ***C*** (same in ***D***, ***E***): 25 μm. IHC: inner hair cells, OHC: outer hair cells, IPhC: inner phalangeal cells, HeC: Hensen's cells, IPC: inner pillar cells, OS: outer sulcus cells, DC1/2: Deiters' cells row 1 or 2, DC3: Deiters' cells row 3, OPC: outer pillar cells, LKO1–3: lateral Kölliker's organ cells groups 1–3, MKO: medial Kölliker's organ cells, IS: inner sulcus cells, IdC: interdental cells, OC90: otoconin 90+ cells.

expression is primarily found at the medial boundary of the cochlear sensory epithelium between E14 and at least P0.

LRRN1 expression switches from inner hair cells to inner phalangeal cells

To confirm smFISH results and to localize LRRN1 expression to specific cell types, immunofluorescence was performed on cochlear whole-mounts, using a commercial polyclonal antibody against the N-terminal portion of human LRRN1. At E14, LRRN1 expression appears as a narrow band extending from the base of the cochlea ~75% to the apex (Fig. 2*A*). Double labeling with the prosensory marker CDKN1B (formerly $p27^{kip1}$) indicates that LRRN1 is localized to the medial edge of the prosensory domain (Fig. 2*A'*). A high-magnification view of the epithelial surface shows $LRRN1^+$ cells forming a single or, in some cases, double row of cells (Fig. 2*B*). Most $LRRN1^+$ cells are negative for surface labeling of CDKN1B, which is an early indicator of HC differentiation as cells exit mitosis (Chen and Segil, 1999; Atkinson et al., 2015). Co-labeling with MYO6, another early hair cell marker, indicates that the majority of $LRRN1^+$ cells at E14 are developing IHCs (Fig. 2*C*). However, some $LRRN1^+$ cells are MYO6 negative. Whether these cells represent immature IPhCs remains undetermined, as definitive markers of IPhCs are not expressed at this stage. Expression of LRRN1 and CADHERIN1 (also known as E-Cadherin), a cell-adhesion protein that is excluded from the medial edge of the prosensory domain (Chacon-Heszele et al., 2012) were also nonoverlapping (Fig. 2*D*). At E16, LRRN1 expression is present along the full length of the cochlear spiral (Fig. 2*E*), and the anti-LRRN1 antibody also labels cells within the spiral ganglion. Examination of cellular expression indicates a transition from IHCs in the apex to IPhCs and the more medial border cells (BCs) in the base (both marked by FABP7; Fig. 2*F*,*G*). In addition, LRRN1-dependent fluorescence intensity indicates a decrease in overall LRRN1 expression along the apical-to-basal gradient. By P1, expression of LRRN1 protein in the cochlea appears to be very low but is detected in apical IPhCs (Fig. 2*H*).

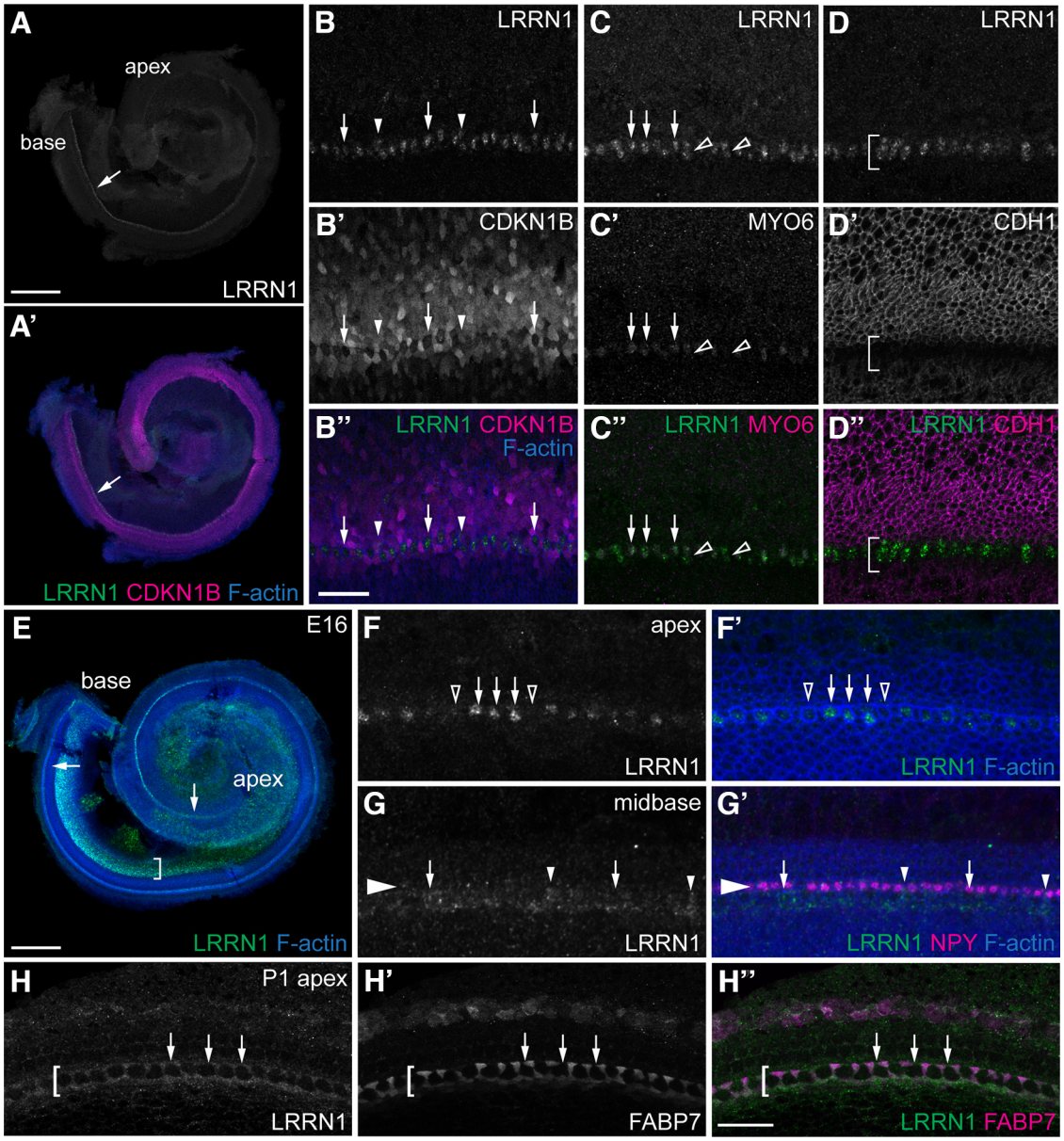

Figure 2. LRRN1 protein is expressed in IHCs and IPhCs/BCs. ***A***, E14 cochlear whole-mount stained with anti-LRRN1 antibody (grayscale). LRRN1 is found in a single row of cells (arrow) extending ~3/4 of the way from the base to apex. ***A'***, Same image as ***A***, showing LRRN1 expression at the medial edge of the prosensory domain, marked by CDKN1B staining. ***B–D***, Confocal Z-stack projections of the surface of the basal region of E14 WT cochleae. ***B***, LRRN1$^+$ cells are mostly negative for surface CDKN1B staining (arrows), but some cells are both LRRN1$^+$ and CDKN1B$^+$ (***B'***, ***B''***, arrowheads). ***C***, Most LRRN1$^+$ cells are also weakly positive for MYO6 (arrows). LRRN1+, MYO6− cells (***C'***, open arrowheads) are often medial to the row of presumptive IHCs and may be developing IPhCs. ***D***, Cadherin-1 (CDH1) is excluded from the medial edge of the prosensory region (bracket), and LRRN1 and CDH1 staining are nonoverlapping. ***E***, E16 whole-mount showing LRRN1 expression along the length of the cochlea (arrows). Anti-LRRN1 signal is also detected in the spiral ganglion (bracket). ***F–H***, Confocal Z-stack projections of the surface of the indicated region from E16 WT cochleae. ***F***, At the apex, LRRN1 is still found in most IHCs (arrows), which have bright phalloidin staining of the cell cortex (***F'***). Some IHCs are not LRRN1+ (open arrowheads). ***G***, LRRN1 in the mid-base is still found medial to the pillar cells, marked by NPY (***G'***, large arrowhead), but anti-LRRN1 staining appears to mainly occur in IPhCs/BCs (arrowheads) though some IHCs are also positive. ***H***, At the P1 apex, LRRN1 staining is weak and mostly overlapping with FABP7 (***H'***) in the IPhCs/BCs (***H''***, brackets). IHCs are LRRN1negative (arrows). Scale bar in ***A***, ***E***, 200 μm; ***B***, ***H***, 20 μm.

Fate-mapping confirms that *Lrrn1*+ prosensory cells predominantly develop as IHCs, IPhCs, and border cells

To definitively identify the fate of *Lrrn1*+ cells, we generated a *Lrrn1-CreERT2* transgenic mouse line (refer to Materials and Methods). *Lrrn1-CreERT2* was crossed to the *Rosa26*^{tdTomato} transgenic reporter (Madisen et al., 2010), and CreERT2 activity was induced by administering tamoxifen at E12 or E16. Cochleae were collected at P0 and labeled for tdTomato, POU4F3 (a HC marker), and FABP7. We observed sparse labeling of *Lrrn1*+ cells in several regions of the cochlea (Fig. 3*A*). A substantial number of mesenchymal cells located beneath the basement membrane were positive for tdTomato, as well as a limited number of cells within the cochlear epithelium (Fig. 3*A*,*B*). Morphologic analysis using high magnification images indicated that tdTomato+ epithelial cells were primarily IHCs, IPhCs, or BCs (Fig. 3*B*). Quantification of *Lrrn1*+ cell fates following Cre-mediated recombination indicates that the vast majority (87.5%, E12 and 90.1%, E16) of all labeled cells develop as cells located along the medial border of the OC (Fig. 3*C*). Of the 61 *Lrrn1*+ cells characterized across both induction stages, the mean percentage of IHCs (18.5), IPhCs (29.5), and border cells (41.0) was far greater than that of Deiters' (2.83) and pillar cells (1.89).

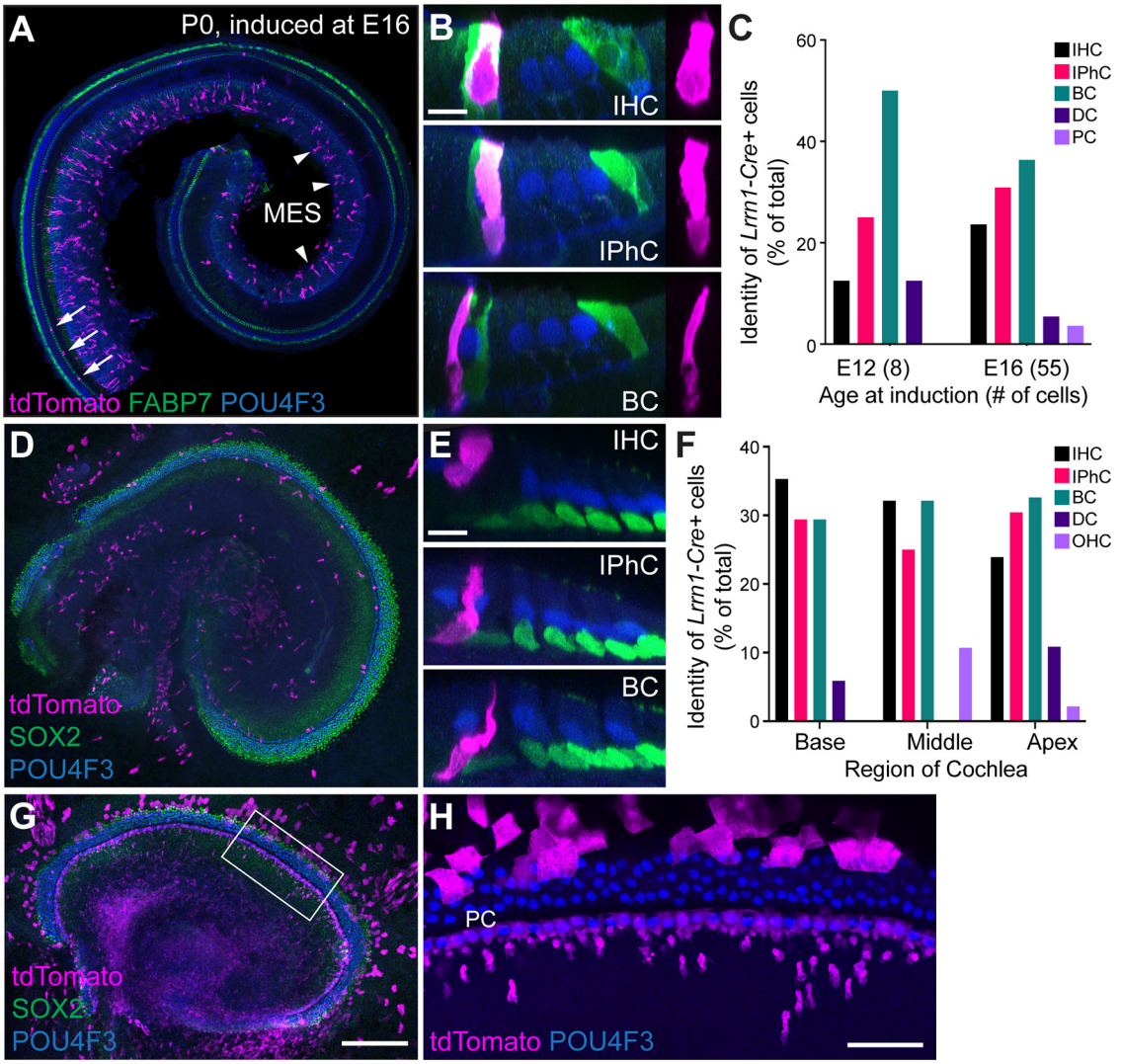

Figure 3. Fate mapping indicates that *Lrrn1*$^{+}$ cells mainly become medial OC cell types. ***A***, Confocal image of *Lrrn1-CreERT2; Rosa26*^{tdTomato} whole-mount cochlea induced *in vivo* at E16. tdTomato^{+} cells (magenta) are present in both periotic mesenchyme (MES; arrowheads) and in the sensory epithelium (marked with anti-FABP7 in green and anti-POU4F3 in blue). Arrows indicate *Lrrn1*+ cells in the sensory epithelium. ***B***, Orthogonal views of *Lrrn1*+ cells in the OC labeled as in ***A***. Examples of an IHC, IPhC, and border cell (BC) are illustrated. Right-hand panels of tdTomato alone illustrate cellular morphology. ***C***, Quantification of *Lrrn1*+ cell types in cochleae induced *in vivo* at E12 ($n = 8$ cells from 4 cochleae) or E16 ($n = 55$ cells from 9 cochleae). Most *Lrrn1*+ cells developed as IHCs, IPhCs, or BCs. A small number of all *Lrrn1*+ cells acquire the lateral fates of pillar cells (2) or Deiters' cells (4), suggesting limited mixing of *Lrrn1*+ cells. ***D***, Low-magnification confocal image of a *Lrrn1-CreERT2; Rosa26*^{tdTomato} cochlear explant established at E14 and induced with 100 nM 4-OH tamoxifen on the day of culture. Explants were fixed and stained after 5 DIV. *Lrrn1*+ cells are in magenta while supporting cells (SOX2) and hair cells (POU4F3) are marked in green and blue, respectively. ***E***, Orthogonal views of the three main *Lrrn1*+ cell types, IHC, IPhC, and BC, from *in vitro* fate mapping. ***F***, Quantification of *Lrrn1*+ cell fates separated by region along the cochlea ($n = 91$ cells from 4 explants). In the apical, middle, and basal regions, most *Lrrn1*+ cells developed as IHCs, IPhCs, or BCs. A small number of *Lrrn1*$^{+}$ Deiters' cells or OHCs (4/91) were observed suggesting minimal cell mixing. ***G***, Confocal image of a *Lrrn1-CreERT2; Rosa26*^{tdTomato} cochlear explant established at E14 and induced at E15 with 1 μM 4-OH tamoxifen and analyzed after 5 DIV, labeled as in ***D***. Note the stripe of magenta cells along the medial edge of the OC. ***H***, Higher magnification of the boxed region in ***G***. *Lrrn1*+ cells form a continuous stripe along the medial edge of the OC, with some positive cells in Kölliker's organ. Scale bar in ***G*** (same in ***A***, ***D***), 200 μm; ***B*** (same in ***E***), 10 μm; ***H***, 50 μm.

Since induction *in vivo* generated a small number of labeled cells within the cochlear epithelium, we sought to induce broader recombination using cochlear explants. Cochleae were dissected at E14 and CreERT2 activity was induced by adding 4-hydroxytamoxifen (4-OH) to the culture media the same day. Explants induced by the addition of 100 nM 4-OH on E14 for 24 h showed levels of recombination similar to those obtained *in vivo* at E16. A significant number of mesenchymal cells were labeled as well as a limited number of cells within the cochlear epithelium (Fig. 3*D*). Consistent with *in vivo* results, analysis of *Lrrn1*+ cell fates *in vitro* indicated that just under 90% of all cells quantified (93) developed as medial cell types (Fig. 3*E*,*F*). To determine whether *Lrrn1*+ cell fates varied according to cochlear region, cell fates were re-analyzed based on their location along the cochlear spiral. In the basal region of the cochlea, over 93% of all *Lrrn1*+ cells developed with medial cell fates. Overall, the majority of *Lrrn1*+ cells developed as supporting cells, a result that contrasted with the observation that many of the LRRN1+ cells in the E14 cochlea appear to be hair cells. This difference is most likely a result of the fact that hair cells differentiate before support cells. It is also possible that the anti-LRRN1 antibody is less sensitive by comparison with either the smFISH or *Lrrn1-CreERT2* fate mapping assays or that there is a delay between expression of mRNA and protein.

By comparison with the base, in the less mature mid and apical regions, the percentage of *Lrrn1*+ cells that developed as medial cell types decreased to ~90% and 88%, respectively (Fig.

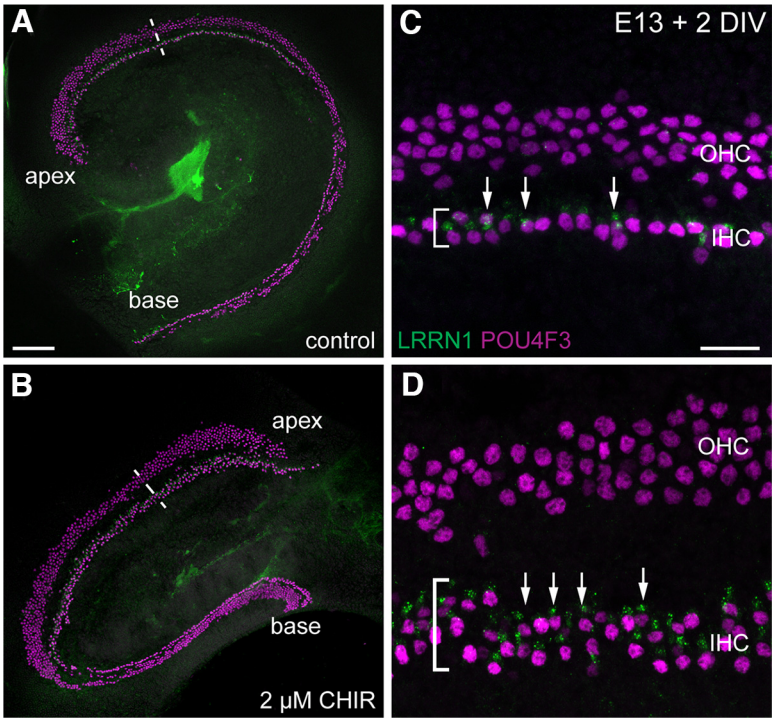

Figure 4. Disruption of the medial-lateral boundary expands LRRN1 expression. ***A–D***, Confocal images of cochlear explants established at E13 and maintained in 0.2% DMSO (control) or 2 μM CHIR99021 for 2 DIV, and then stained for LRRN1 and POU4F3. ***A***, Control explant has mostly normal morphology of one to two rows of POU4F3+ IHCs. ***B***, CHIR-treated explant has additional IHCs and a wide gap between IHCs and OHCs. ***C***, View of the mid-apical region of the explant in ***A***. POU4F3+ IHCs (bracket) are also LRRN1+ (arrows). ***D***, Same as ***C*** for the explant in ***B***. Many more POU4F3+ cells are found in the expanded IHC region (bracket), and there is a corresponding increase in LRRN1+ cells. Scale bar in ***A*** (same for ***B***), 100 μm; ***C*** (same for ***D***), 20 μm.

3*F*). Since the smFISH analysis indicated that all *Lrrn1*+ cells at E14 are located at the medial edge of the prosensory domain, these results suggest that some cell movement across the medial-lateral boundary of the OC may occur. However, this effect may also be a result of patterning defects that are known to occur *in vitro*.

Finally, to generate a more comprehensive understanding of the fates of *Lrrn1*+ cells, explants were established at E14 and induced for 24 h beginning on the equivalent of E15 with 1 μM 4-OH. This higher level of induction resulted in a labeled stripe (not quantified) of cells at the medial edge of the epithelium that includes nearly all IHCs, IPhCs and BCs (Fig. 3*G*). Yet while only sporadic *Lrrn1*+ cells developed with lateral cell fates (pillar cells, OHCs, Deiters' cells), multiple cells located in Kölliker's organ were also labeled (Fig. 3*G*,*H*). To determine whether this result could represent an artifact of the culture system or ectopic recombination because of infidelity in expression of the *Lrrn1-CreERT2* transgenic, we examined *Lrrn1* expression in a recently published single-cell RNAseq dataset for cochlear epithelial cells at E16 and found that *Lrrn1* is expressed in a small number of cells located in Kölliker's organ (Kolla et al., 2020), and some signal is also detected in these cells by smFISH (Fig. 1*D*). Overall, these results are consistent with expression of *Lrrn1* being largely, but not entirely, restricted to cells at the medial boundary of the developing organ of Corti, a bias that is stronger in the more differentiated basal region at any specific time point.

Lrrn1 expression is regulated through medial-lateral patterning

Expression of LRRN1 is mostly restricted to cells located at the medial boundary of the OC, suggesting that Lrrn1 expression could be regulated through specification of the medial-lateral cochlear axis. An early developmental gradient of BMP4, originating at the extreme lateral edge of the cochlear duct, is thought to act as a morphogen that specifies this axis (Ohyama et al., 2010). To determine whether LRRN1 expression is regulated through this patterning mechanism, cochlear explants were established at E13, and specification of the medial-lateral axis was disrupted by treating explants with CHIR99021 (CHIR), a GSK3 antagonist, that downregulates Bmp4 signaling in the cochlea (Ellis et al., 2019). Explants treated with CHIR develop multiple rows of IHCs, BCs, and IPhCs, in part through expansion of the medial OC (Ellis et al., 2019). Labeling of CHIR-treated explants with the HC marker anti-POU4F3 and anti-LRRN1 indicated an expansion in LRRN1 expression that paralleled its expansion in the IHC region (Fig. 4*A–D*). These results demonstrate that expression of LRRN1 is regulated by the same factors that specify the medial-lateral cochlear axis. Whether *Lrrn1* is a direct target of Bmp4 signaling or is indirectly influenced by an intermediate factor remains to be determined.

The medial boundary of the OC is disrupted in *Lrrn1* mutant mice

To determine whether *Lrrn1* plays a role in cochlear development, we used TALEN-mediated mutagenesis to target the 10th LRR repeat in *Lrrn1*. Three different lines were generated using different targeting sequences (see Materials and Methods), resulting in 2-, 4-, or 31-bp deletions within the *Lrrn1* gene. The resulting frameshifts and truncations are predicted to generate large N-terminal extracellular fragments which likely act as loss-of-function mutations (Fig. 5*A*,*B*). All three lines showed phenotypically and statistically similar cochlear phenotypes so data and images from all three lines were merged for experimental analysis, and mutants are referred to as *Lrrn1*$^{-/-}$. Immunolabeling of cochleae from embryos with either the 2- or 4-bp *Lrrn1* deletion with anti-LRRN1 antibody indicated no labeling, consistent with an absence of full-length LRRN1 (Fig. 5). At E14, LRRN1 staining in the base of a *Lrrn1*$^{+/-}$ cochleae co-localizes with POU4F3 in a single row of developing IHCs, but no LRRN1 signal is apparent in the *Lrrn1* mutant (Fig. 5*C–F*). Similarly, at E15, LRRN1 protein is detected in a *Lrrn1*$^{+/-}$ section at the medial edge of the sensory epithelium, but not in a *Lrrn1*$^{-/-}$ section (Fig. 5*G–J*). The lack of detectable anti-LRRN1 staining in *Lrrn1*$^{-/-}$ tissue suggests these truncating mutations generate null alleles of *Lrrn1*.

Lrrn1$^{-/-}$ male and female mice are viable and fertile with no obvious gross developmental defects. *Lrrn1*$^{+/-}$ heterozygous animals showed no differences from wild-type and, therefore, were used as littermate controls. Examination of the cochleae from *Lrrn1*$^{-/-}$ and *Lrrn1*$^{+/-}$ mice at P0 indicated a significant increase in the number of IHC doublets along the length of the epithelium in *Lrrn1*$^{-/-}$ animals (Fig. 6*A*). To determine whether these additional IHCs represented a phenotypic conversion of adjacent supporting cells into hair cells or resulted from a change in the boundary between sensory and nonsensory regions of the

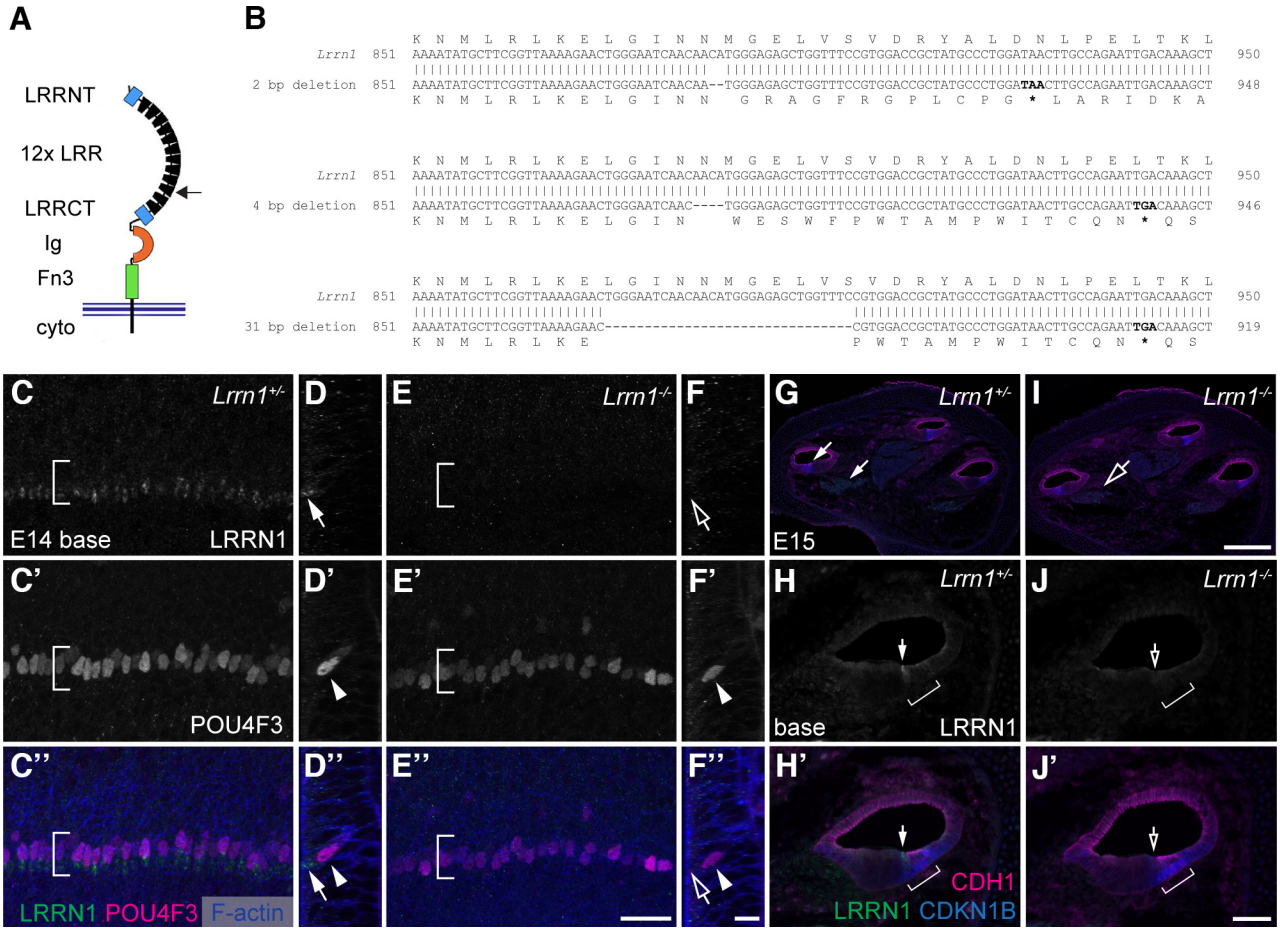

Figure 5. TALEN-mediated mutagenesis of *Lrrn1* results in loss of LRRN1 protein. ***A***, Schematic of the protein structure of LRRN1. LRRN1 contains leucine-rich N-terminal and C-terminal domains (LRRNT and LRRCT, blue boxes), 12 leucine-rich repeats (LRR, black boxes), an immunoglobulin domain (Ig, orange crescent), a fibronectin Type III domain (Fn3, green box), a transmembrane domain, and a short C-terminal cytoplasmic tail. The 10th LRR was targeted for TALEN-mediated mutagenesis (arrow). ***B***, Deletions in the genomic sequence of *Lrrn1* of 2, 4, or 31 bp. All three deletions result in frameshifts predicted to generate truncated LRRN1 proteins. ***C***, ***D***, Confocal Z-stack projections of the basal region of E14 WT cochleae. ***C***, Surface view of LRRN1+ cells in a $Lrrn1^{+/-}$ cochlea forming a single row, overlapping with developing HCs marked by POU4F3 (bracket). ***D***, Orthogonal view from ***C***. LRRN1 is localized to the luminal surface of the cell (arrow), above the POU4F3+ nucleus (arrowhead). ***E***, ***F***, Similar views to ***C***, ***D*** from a $Lrrn1^{-/-}$ cochlea. POU4F3+ cells are still present (bracket, arrowhead), but LRRN1 signal is absent (open arrow). ***G–J***, Confocal images of cryosections through $Lrrn1^{+/-}$ or $Lrrn1^{-/-}$ cochlear ducts at E15. ***G***, LRRN1 staining is found in the OC and the spiral ganglion (arrows). ***H***, LRRN1 at the base appears to be expressed in a single cell (arrow) at the medial edge of the OC (bracket), marked by CDH1 and CDKN1B (***H'***). ***I***, No anti-LRRN1 staining is found in the OC of a *Lrrn1* mutant cochlea, but faint signal is present in the spiral ganglion, probably representing background staining, which may contribute to the LRRN1 signal found in Figure 2*E*. ***J***, No LRRN1 signal is present in a basal section of a $Lrrn1^{-/-}$ cochlea. Scale bar in ***E*** (same for ***C***), 20 μm; ***F*** (same for ***D***), 10 μm; ***I*** (same for ***G***), 200 μm, ***J*** (same for ***H***), 50 μm.

cochlear duct, IPhCs and BCs were labeled with anti-FABP7. We observed an increased number of IPhC/BCs, suggesting a change in the sensory/nonsensory boundary (Fig. 6*B*). Quantification of the number of additional IHCs and IPhC/BCs in basal, mid, and apical regions along the cochlear spiral indicates significant increases in both cell types at each position (Fig. 6*C*). The *Lrrn1* mutant phenotype is more pronounced in the apical region, an effect that may be attributed to the late maturation of the apical OC and its corresponding susceptibility to developmental mutations (Fig. 6*C*).

Patterning defects, including IHC doublets, can also occur because of inhibition of cochlear outgrowth. To determine whether the phenotype observed in *Lrrn1* mutants is a result of outgrowth defects, the density of normally aligned IHCs and OHCs and the total length of the cochlear duct were determined for $Lrrn1^{+/-}$ and $Lrrn1^{-/-}$ cochleae at P0 (Fig. 6*D*,*E*). No significant changes in either cochlear length or hair cell density were found, suggesting that cochlear outgrowth is unaffected in the absence of *Lrrn1*. Finally, we examined patterning of pillar cells and Deiters' cells in $Lrrn1^{-/-}$ cochlea, both of which were indistinguishable from control (Fig. 6*F*,*G*).

To determine when the initial appearance of the patterning defect occurs in *Lrrn1* mutants, E14 cochleae were labeled with anti-DLL1, an early marker of IHCs, and CDKN1B, a marker of the prosensory domain. In controls, a single row of $DLL1^{+}$ cells was present at the medial edge of the prosensory domain (Fig. 6*H*). In contrast, in $Lrrn1^{-/-}$ cochleae, doublets of IHCs were already present (Fig. 6*H*, arrows). These results suggest that specification of the medial boundary of the prosensory domain is disrupted early in *Lrrn1* mutant OC development.

In some cases, additional medial OC cells can arise because of a delay in cell cycle exit of prosensory cells (Prajapati-DiNubila et al., 2019). To determine whether an increase in proliferation contributed to the formation of ectopic IHCs and SCs in *Lrrn1* mutants, we examined the expression of the proliferation marker Ki67 at E14, the earliest stage that *Lrrn1* expression is detected. Ki67 should normally be excluded from the prosensory domain as cells exit the cell cycle between E12 and E14 (Chen and Segil,

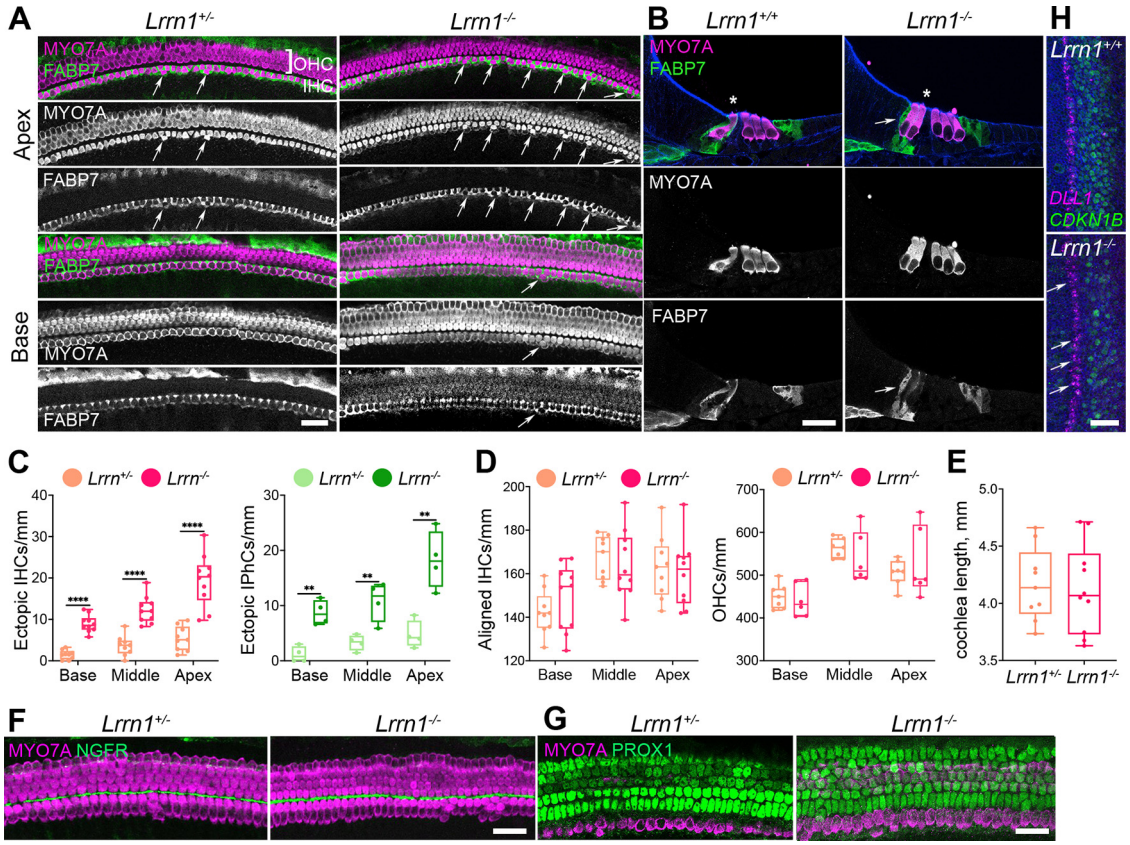

Figure 6. The medial boundary of the organ of Corti is disrupted in *Lrrn1* mutants. ***A***, Surface images of the apical (top) and basal (bottom) regions of the OC from $Lrrn1^{+/-}$ and $Lrrn1^{-/-}$ mice at P0. $Lrrn1^{+/-}$ cochleae have a single row of IHCs (MYO7A, magenta) with surrounding IPhCs (FABP7, green). Two ectopic IHCs (arrows) are present in the apical region. $Lrrn1^{-/-}$ cochleae show a significantly increased number of ectopic IHCs (arrows) in both apical and basal regions, and the vast majority of IHCs are surrounded by ectopic IPhCs. ***B***, Cross-sections through the OC from the basal region of $Lrrn1^{+/+}$ and $Lrrn1^{-/-}$ cochleae at P0. Asterisk in each upper panel marks the endogenous IHC. Note the presence of an additional IPhC (arrow in lower panel) adjacent to the ectopic IHC in the *Lrrn1* mutant. ***C***, The number of ectopic IHCs and IPhCs is significantly increased in all three regions of the cochlea in *Lrrn1* mutants ***D***, In contrast, the number of aligned IHCs and OHCs did not differ significantly between $Lrrn^{+/-}$ and $Lrrn1^{-/-}$ cochleae. *N* for each genotype: $Lrrn1^{+/-}$, 9, $Lrrn1^{-/-}$, 10 (IHCs, OHCs); $Lrrn1^{+/-}$, 4, $Lrrn1^{-/-}$, 4 (IPhCs). ***E***, No significant difference in cochlear length between $Lrrn1^{+/-}$ ($N = 9$) and $Lrrn1^{-/-}$ ($N = 10$) cochleae. ***F***, Surface views from the middle region of cochleae from mice with the indicated genotypes. Anti-NGFR labels inner pillar cells which appear similar in both samples. ***G***, Similar view as in ***F***, but from cochleae labeled with anti-MYO7A and anti-PROX1 which labels nuclei of pillar and Deiters' cells. Plane of focus is at the level of the SC nuclei. PROX1 expression appears comparable between $Lrrn1^{+/-}$ and $Lrrn1^{-/-}$. ***H***, Labeling with anti-DLL1 (magenta), an early marker of IHCs, in the base of the cochlea at E14. In control a single line of $Dll1^{+}$-IHCs is present while in the *Lrrn1* mutant several ectopic IHCs are already present (arrows). $^{****}p < 0.0001$, $^{**}p < 0.01$, Scale bars for all, 25 µm.

1999). Within the prosensory domain, marked by overlapping expression of CDKN1B and SOX2 (Driver et al., 2017), we found a total of 4 Ki67+ cells in 8 $Lrrn1^{+/-}$ cochleae, and 4 Ki67+ cells in 10 $Lrrn1^{-/-}$ cochleae. While we cannot rule out that a modest increase in proliferation may contribute to the extra medial cells observed in *Lrrn1* mutants, it does not appear to be a significant factor.

Lrrn1 genetically interacts with *Notch1* to mediate medial boundary formation

The disrupted medial boundary phenotype in *Lrrn1* mutant cochleae strongly resembles the cochlear phenotype described in response to mild disruption of Notch signaling during the same developmental period (Basch et al., 2016). Moreover, *Lrrn1* has been reported to interact with the Notch signaling pathway in other developing systems (Andreae et al., 2007; Tossell et al., 2011). These results suggest that the cochlear phenotype in *Lrrn1* mutants could be a result of modulation of the Notch pathway during medial boundary formation. To test this hypothesis, we generated an allelic series of different *Notch1* and *Lrrn1* deletions. In agreement with previous results (Zhang et al., 2000), $Notch1^{+/-}$ cochleae showed no significant increase in IHC doublets at P0 (Fig. 7*A*,*B*). IHC doublets were also not significantly increased in $Lrrn1^{+/-}$; $Notch1^{+/-}$ cochleae, despite the increased variability of the phenotype (Fig. 7*A*,*B*). Consistent with the findings described for the *Lrrn1* mutant, a significant increase in IHC doublets was observed in $Lrrn1^{-/-}$; $Notch1^{+/+}$ cochleae compared with $Lrrn1^{+/-}$ littermates. However, the number of doublets was further, and statistically significantly, increased in $Lrrn1^{-/-}$; $Notch1^{+/-}$ animals relative to $Lrrn1^{-/-}$; $Notch1^{+/+}$ mice (Fig. 7*A*,*B*). These results are consistent with a genetic interaction between *Notch1* and *Lrrn1* and suggest that Lrrn1 normally acts to enhance Notch1 signaling.

If Lrrn1 does augment Notch signaling, then another potential phenotype in $Lrrn1^{-/-}$; $Notch1^{+/-}$ cochleae would be an increase in the number of IHCs aligned directly adjacent to pillar cells, as Notch1 has been shown to inhibit IHC formation (Lanford et al., 1999; Kiernan et al., 2005). To test this hypothesis, the number of aligned IHCs was determined for each genotype in the allelic series. In accordance with the expected reduction of Notch1 activation along the medial border, results indicated a significant increase in the number of aligned IHCs only in $Lrrn1^{-/-}$; $Notch1^{+/-}$ cochleae (Fig. 7*C*), while the length of the cochleae was statistically unchanged (data not shown). Higher magnification of labeled hair cells revealed noticeably

smaller IHC surface areas in *Lrrn1*$^{-/-}$; *Notch1*$^{+/-}$ animals (Fig. 7*D*), a result that was confirmed quantitatively (Fig. 7*E*,*F*). Overall, these phenotypes support the hypothesis that decreased Notch1 signaling in the absence of Lrrn1 leads to both increased boundary disruptions and IHC formation.

Absence of *Lrrn1* enhances the effects of γ-secretase inhibition in cochlear explants

To examine the regulation of Notch signaling by Lrrn1 more directly, we asked whether the absence of *Lrrn1* leads to increased sensitivity to the potent Notch inhibitor LY411575 (Mizutari et al., 2013). Cochlear explants from WT mice were established at E14 and treated with different dosages of LY411575 to determine the maximum concentration of LY411575 that did not cause an increase in IHC numbers relative to untreated controls (500 pM; Fig. 8*A*,*B*). Next, cochlear explants from *Lrrn1*$^{+/+}$, *Lrrn1*$^{+/-}$, and *Lrrn1*$^{-/-}$ mice were established at E14 and treated with 500 pM LY411575 for 2 d *in vitro* (DIV), equivalent to E14–E16, then maintained for an additional three DIV. An increased frequency of IHC doublets was observed in *Lrrn1*$^{-/-}$ explants treated with LY411575 relative to both control explants treated with LY411575 and to untreated *Lrrn1*$^{-/-}$ cochleae (Fig. 8*A*,*B*). Quantification of IHC density indicated a significant increase in *Lrrn1*$^{-/-}$ explants treated with LY411575, relative to both untreated *Lrrn1*$^{-/-}$ explants and to *Lrrn1*$^{+/+}$ explants treated with LY411575 (Fig. 8*C*).

As a final examination of the effects of *Lrrn1*deletion on Notch signaling, smFISH was used to examine the expression of Notch pathway genes. In mice with deletion of both *Manic fringe* (*Mfng*) and *Lunatic fringe* (*Lfng*), a similar duplication of medial cochlear sensory cells has been observed (Basch et al., 2016). We did not detect any difference in expression of either *Mfng* or *Lfng* in E15 *Lrrn1*$^{-/-}$ cochleae compared with *Lrrn1*$^{+/-}$ (Fig. 8*D*,*E*), or in the Notch ligand JAG1 (Fig. 8*F*–*G*'). Deletion of the transcription factor *Hes1,* a Notch target and effector, also leads to an expansion of IHCs and medial SCs (Zine et al., 2001; Tateya et al., 2011). At the base of the E15 cochlea, *Hes1* is normally expressed in a strong, narrow stripe lateral to the OHCs, and a more diffuse domain medial to the IHCs (HCs labeled with MYOSIN6; Fig. 8*H*). While lateral *Hes1* expression was unchanged in *Lrrn1*$^{-/-}$ cochleae, the medial *Hes1* signal appeared to be reduced (Fig. 8*I*). To quantify the change in *Hes1*, we compared the ratios of medial to lateral *Hes1* intensity in *Lrrn1*$^{+/+}$ and *Lrrn1*$^{-/-}$ samples and found that medial *Hes1* intensity was significantly reduced in *Lrrn1* mutant cochleae (Fig. 8*J*). Overall, these results are consistent with decreased Notch activation in *Lrrn1* mutants, suggesting that from its position at the medial boundary, Lrrn1 typically enhances Notch signaling in adjacent nonsensory cells, an effect that may be mediated through *Hes1* expression.

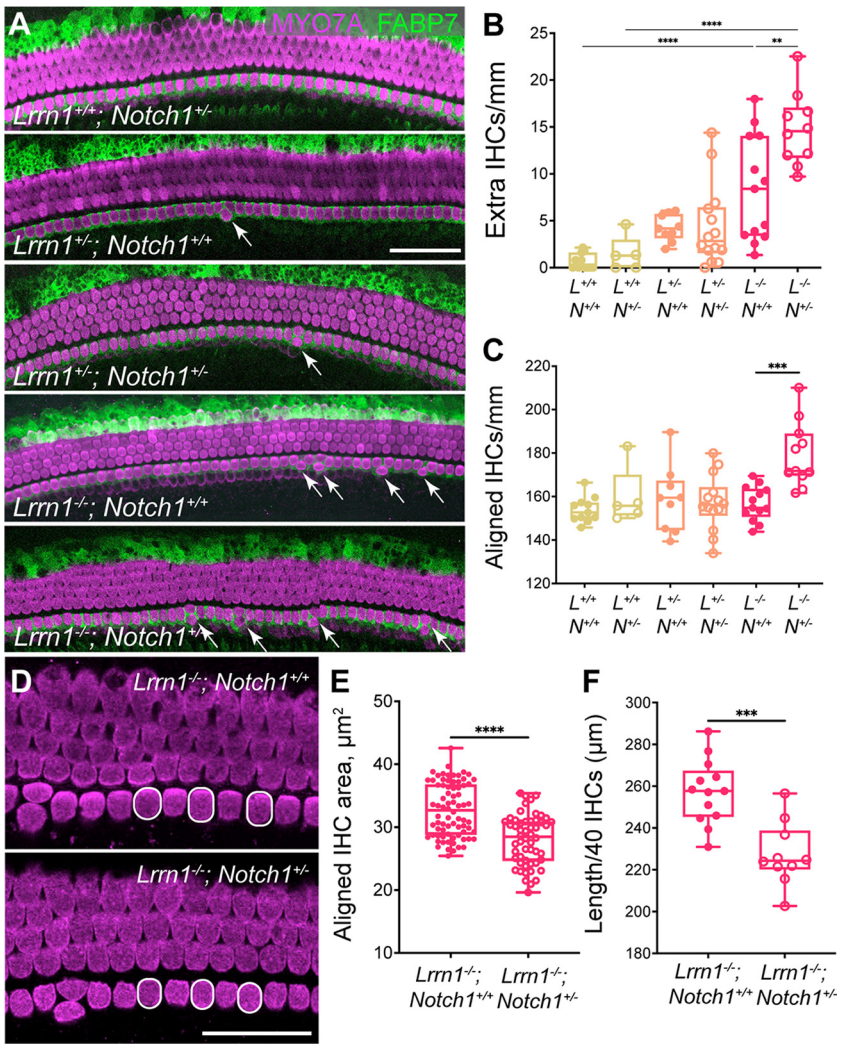

Figure 7. *Lrrn1* interacts genetically with *Notch1* to mediate medial boundary formation. ***A***, Representative surface images of the middle turns from P0 cochleae with the indicated genotypes. HCs are labeled with anti-MYO7A and SCs are labeled with anti-FABP7. Increased IHC doublets and corresponding supporting cells are observed in *Lrrn1*$^{-/-}$; *Notch1*$^{+/+}$ and *Lrrn1*$^{-/-}$; *Notch1*$^{+/-}$ genotypes. ***B***, Number of extra IHCs per genotype, calculated per mm based on the total number of extra IHCs in the middle region of each sample. The *Lrrn1* genotype underlies greater than half (51.6%) of the total variation between samples while only a small fraction of this variation may be attributed to the *Notch1* genotype (3.90%). The mean number of extra IHCs does not differ significantly between *Lrrn1*$^{+/+}$ (0.64, 1.45) and *Lrrn1*$^{+/-}$ (4.22, 4.37) cochleae in the *Notch1*$^{+/+}$ versus *Notch1*$^{+/-}$ background. Heterozygosity at the *Notch1* locus induces a significant increase in the mean number of IHC doublets in *Lrrn1* mutants (8.37–14.7). ***C***, In addition to increased IHC doublets, *Lrrn1*$^{-/-}$; *Notch1*$^{+/-}$ cochleae also have a significant increase in endogenous IHCs (157–179). ***D***, Surface view of cochleae from the indicated genotypes. Circles illustrate decreased endogenous IHC surface area in *Lrrn1*$^{-/-}$; *Notch1*$^{+/-}$ cochleae, possibly underlying the increased number of cells. ***E***, ***F***, Quantification of endogenous IHC luminal surface area and hair cell packing indicate a significant reduction in cell surface area (4.74 ± 0.729 µm^2) and a significantly greater density (29.9 ± 6.41 µm/40 cells) of IHCs in *Lrrn1*$^{-/-}$; *Notch1*$^{+/-}$ cochleae. ****$p < 0.0001$, ***$p < 0.001$, **$p < 0.01$, *N* for each genotype: (*Notch1*$^{+/+}$ background) *Lrrn1*$^{+/+}$, 11, *Lrrn1*$^{+/-}$, 9, *Lrrn1*$^{-/-}$, 10; (*Notch1*$^{+/-}$ background) *Lrrn1*$^{+/+}$, 5, *Lrrn1*$^{+/-}$, 14, *Lrrn1*$^{-/-}$, 10. Scale bar in ***A***, 50 µm; ***D***, 25 µm.

Discussion

Straight cellular boundaries within populations of epithelial cells often specify signaling centers that influence unique cell fates on one or both sides of the boundary (Wurst and Bally-Cuif, 2001; Wang and Dahmann, 2020). The OC contains at least three boundaries: a

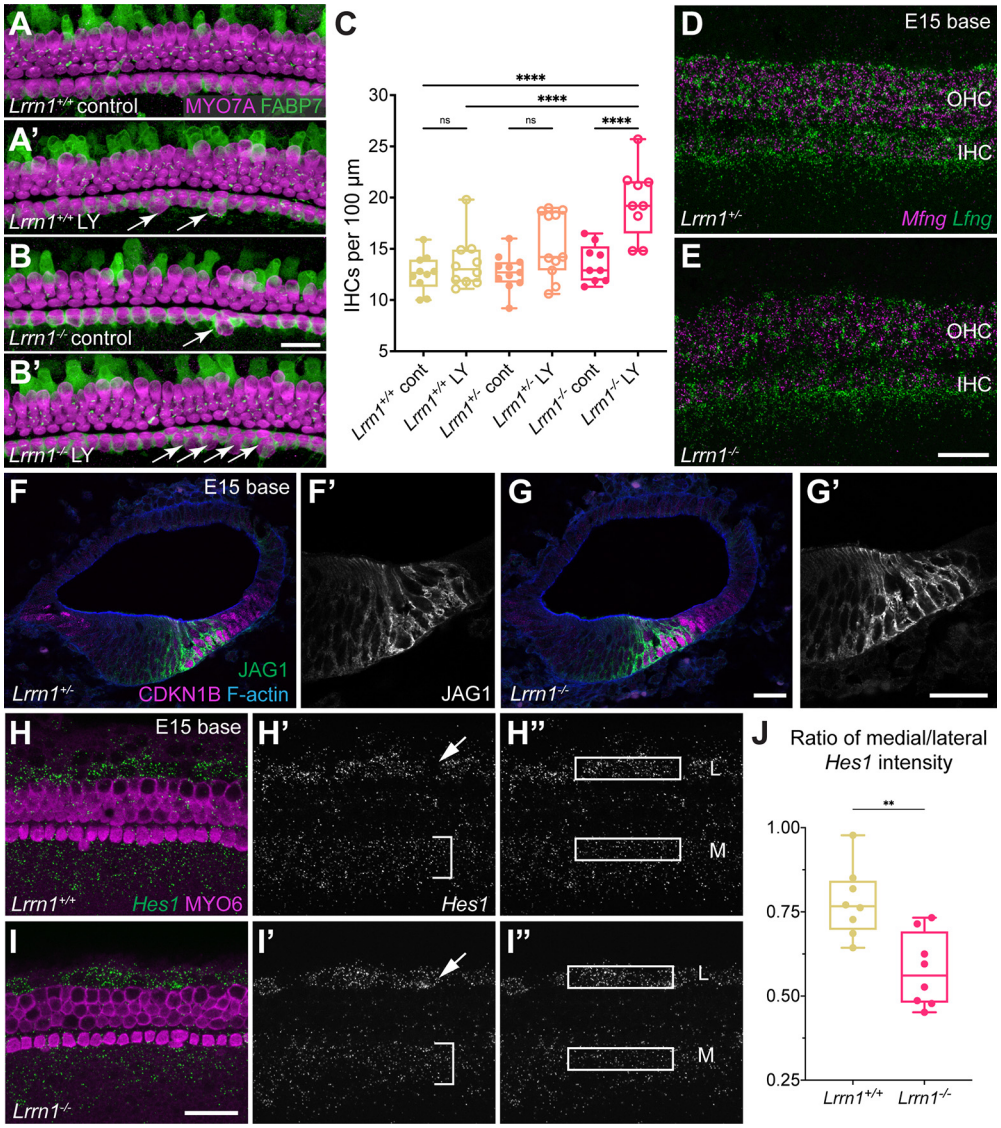

Figure 8. *Lrrn1* mutants show disruptions to Notch signaling. ***A***, Surface views of the middle regions from cochlear explants established on E14 and maintained in 0.2% DMSO (control) or 500 pM LY411575 (LY) for 2 DIV, then in control media for an additional 3 DIV. MYO7A+ HCs, magenta, FABP7+ IPhCs, green. Occasional IHC doublets (arrows) are observed in $Lrrn1^{+/+}$ explants treated with LY (***A'***) and in $Lrrn1^{-/-}$ control explants (***B***). However, significantly more doublets are observed in LY-treated $Lrrn1^{-/-}$ explants (***B'***). ***C***, Density of both aligned and ectopic IHCs for cochlear explants maintained in the indicated conditions. Density in $Lrrn1^{+/+}$ or $Lrrn1^{+/-}$ explants treated with LY was unchanged from control explants of the same genotype ($p = 0.99, 0.19$), but was significantly increased in LY-treated $Lrrn1^{-/-}$ explants versus untreated $Lrrn1^{-/-}$ explants. LY treatment of $Lrrn1^{-/-}$ explants induced a significant increase in IHC density by comparison with control or LY-treated wild-type explants (****$p < 0.0001$, n.s., not significant). *N* for each genotype, both conditions: $Lrrn1^{+/+}$, 10, $Lrrn1^{+/-}$, 11, $Lrrn1^{-/-}$, 9. ***D***, ***E***, Confocal Z-stack projection of the surface view of whole-mount smFISH for *Mfng* (magenta) and *Lfng* (green) in the basal region of E15 cochleae. No difference was observed between $Lrrn1^{+/-}$ and $Lrrn1^{-/-}$. ***F***, ***G***, Sections of the E15 cochlear base showing JAG1 staining (green) in the differentiating OC, also marked by CDKN1B (magenta). JAG1 appears similar in $Lrrn1^{+/-}$ (***F***) and $Lrrn1^{-/-}$ (***G***) cochleae. ***F'***, ***G'*** JAG1 in SCs in the developing OC (grayscale). ***H***, ***I***, smFISH for *Hes1* (green) shown in a confocal Z-stack projection near the surface of the cochlear base at E15. Differentiating HCs are stained with anti-MYO6 (magenta). The intensity of the lateral *Hes1* signal (***H'***, ***I'***, arrows) is equivalent in $Lrrn1^{-/-}$ to wild-type, but medial *Hes1* is reduced (brackets). ***H''***, ***I''***, Boxes showing the ROIs used to compare the intensity of the *Hes1* smFISH signal. L, lateral; M, medial. ***J***, Average pixel intensity of medial *Hes1* signal, normalized to the paired lateral ROI. Medial *Hes1* is significantly reduced in $Lrrn1^{-/-}$ cochleae (**$p = 0.002$). $N = 8$ paired (medial + lateral) ROIs from 4 cochlea of each genotype. Scale bar in ***B*** (same for ***A***), 25 µm; ***E*** (same for ***D***), 20 µm; ***G***, ***G'*** (same for ***F***, ***F'***), 25 µm, ***I*** (same for ***H***), 20 µm.

medial boundary between the single rows of IHCs/IPhCs/BCs and adjacent nonsensory cells (Basch et al., 2016), a similar lateral sensory/nonsensory boundary between the third row of Deiters' cells and nonsensory cells (Ohyama et al., 2010), and a boundary between IHCs and pillar cells. Two of these, the medial sensory/nonsensory and the IHC/pillar cell boundaries, are characterized by a straight, highly organized alignment of unique cell types on each side (Driver and Kelley, 2020). The lateral interface between sensory and nonsensory cells, while also organized, is less regular and can feature deviations in alignment. Our understanding of how these boundaries are formed remains limited.

A likely first step in the creation of the OC boundaries is establishment of the medial-lateral axis of the cochlear duct. BMP4 expression in the lateral region of the cochlea has been proposed to create a morphogen gradient that specifies cellular identities along this axis (Ohyama et al., 2010; Munnamalai and Fekete, 2016). Deletion of the BMP receptors *Alk3* and *Alk6* within the duct leads to an expansion of Kölliker's organ at the expense of the outer sulcus (Ohyama et al., 2010). While morphogen gradients play key roles in specifying differing cellular identities (Bier and De Robertis, 2015; Irizarry and Stathopoulos, 2021), the dynamic nature of diffusive processes, especially at

increased distance from the source, makes precisely positioning a straight boundary from a morphogen gradient alone difficult (Lander, 2007). Counter gradients of FGF10 or an unidentified WNT may act with BMP4 to improve spatial resolution, but data to support this hypothesis have been inconsistent (Urness et al., 2015; Munnamalai and Fekete, 2016; Ellis et al., 2019).

Work from Basch et al. (2016) examined cell-cell interactions at the medial prosensory/nonsensory boundary. Based on transient expression of *Atoh1*, *Jag2*, *Dll1*, *Lfng*, and *Mfng* in cells located along this boundary, they suggested that a peak of hair cell-inducing factors at the medial edge of the prosensory domain directs upregulation of the above genes. Differences in Notch signaling then arise as a result of various *cis(-)* and *trans*-interactions of Notch ligands and receptors. The negative feedback loop between expression of Notch and Notch ligands leads to a difference in activity (higher in medial nonsensory cells, lower in lateral prosensory cells) which specifies the medial boundary through inhibition of prosensory induction (Hartman et al., 2010; Pan et al., 2010, 2013).

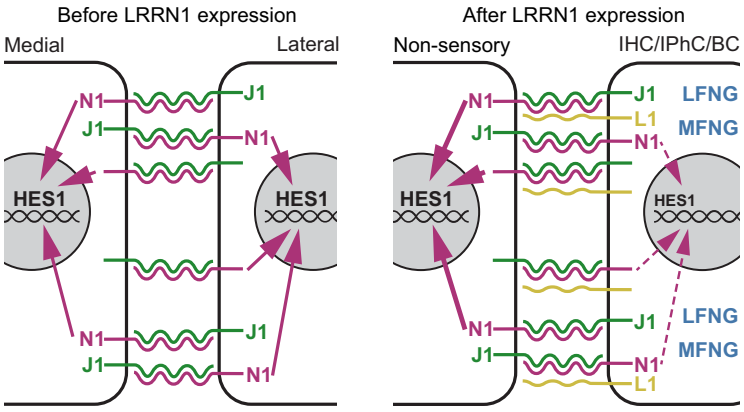

Figure 9. Model of cellular interactions at the developing cochlear medial boundary. Left panel, Before *Lrrn1* expression at E14, cells on both side of the boundary express roughly equal levels of Notch1 (N1) and the Notch ligand Jagged1 (J1) leading to roughly equivalent levels of Notch activation and expression of the Notch target *Hes1*. Right panel, Because of differences in positional identity, cells on one side of the boundary begin to express Lunatic Fringe (Lfng), Manic Fringe (Mfng), and Lrrn1 (L1). Lfng and Mfng glycosylate Jagged1, leading to decreased autocrine Notch signaling, while expression of Lrrn1 enhances Notch activation in neighboring cells. This results in heterogeneous levels of Notch pathway activation. More medial cells are prevented from assuming a sensory cell fate by the increased level of Notch activity.

Consistent with this hypothesis, deletion of *Lfng* and *Mfng,* resulting in decreased Notch signaling to medial nonsensory cells across the boundary, causes duplication of both IHCs and IPhCs (Basch et al., 2016). The increase in both cell types is key, as it distinguishes a change in the boundary from a defect in lateral inhibition, in which the increase in hair cells comes at the expense of supporting cells (Kiernan et al., 2005). Similar defects in medial boundary formation are observed in *Jag1* heterozygotes and in other mutants that decrease, but do not abolish, Notch signaling (Kiernan et al., 2001; Zine et al., 2001; Brooker et al., 2006). These results demonstrate roles for Notch1, Jag1, Lfng, and Mfng in boundary formation. However, a central premise of the hypothesis proposed by Basch et al. (2016) is that Lfng and Mfng enhance signaling by the Dll1 ligand. Two observations argue against an exclusive role for Dll1 in boundary formation. First, Dll1 is only expressed in hair cells, while the boundary includes hair cells and supporting cells. Second, while the phenotype has not been thoroughly examined, images of the medial boundary from *Dll1* mutant mice seem more consistent with impaired lateral inhibition rather than disrupted boundary formation. *Dll1* mutants include examples of what appear to be IHCs touching each other (Kiernan et al., 2005; Brooker et al., 2006), and Jag1 labeling in *Dll1* mutant cochleae did not indicate an increased number of IPhCs or BCs (Brooker et al., 2006). These results suggest that other factors interact with or directly modulate Notch activity in cells on one side or the other of the medial boundary.

In this study, we demonstrate that the timing and location of *Lrrn1* expression coincides with the formation of the medial boundary (Basch et al., 2016). Lrrn1 has been shown to regulate Notch activity across boundaries in developmental and cancerous contexts (Tossell et al., 2011; Y. Zhang et al., 2021) and our data imply a similar role in the cochlea. Disruptions in medial boundary formation occur in response to weakened, not absent, Notch signaling (Basch et al., 2016). Using multiple approaches, we demonstrated that the loss of Lrrn1 decreases Notch signaling, leading to duplications at the medial boundary. As illustrated in Figure 9, these results suggest that Lrrn1 expression in developing prosensory cells likely acts to augment Jag1-mediated induction of the Notch target gene *Hes1* in adjacent nonsensory cells, an interaction that is supported by recent findings from a study of pancreatic carcinoma (Y. Zhang et al., 2021). However, while unlikely, we cannot completely rule out the possibility that Lrrn1 acts via a separate, parallel pathway that simultaneously regulates medial boundary formation. The demonstrated decrease in *Hes1* is consistent with modulation of Notch signaling, but whether this is the primary effector of Lrrn1 signaling could only be demonstrated definitively by restoring *Hes1* expression to WT levels in a *Lrrn1* mutant background.

The mechanisms by which Lrrn1 enhances Notch activity in neighboring cells is unclear. Previous studies examining the role of Lrrn1 during formation of the chick midbrain/hindbrain boundary demonstrated that Lrrn1 induces autocrine expression of Lfng (Tossell et al., 2011), prompting Lfng-mediated glycosylation and enhancement of transcellular Notch signaling (Panin et al., 1997; Brückner et al., 2000; Moloney et al., 2000). However, no change in expression of *Lfng* or *Mfng* was observed in $Lrrn1^{-/-}$ cochleae. An alternative mechanism is through a direct interaction of Lrrn1 with Notch or Notch ligands in the same or adjacent cells. Lrrn1 is a transmembrane protein with an extracellular leucine-rich repeat domain (Taguchi et al., 1996; Andreae et al., 2007) and the *Drosophila* homologs Tartan and Capricious have been shown to confer differential adhesion through transcellular binding (Milán et al., 2001; Mao et al., 2008). Therefore, interactions with Notch, Notch ligands, or other extracellular molecules could lead to modulation of Notch signaling. While Notch1 has not been reported to interact physically with Lrrn1 or other leucine-rich repeat molecules, a small leucine-rich proteoglycan, Biglycan, has been shown to bind to Notch3 (X. Zhang et al., 2015), suggesting possible physical interactions that could modulate Notch signaling.

The restricted expression of Lrrn1 to a narrow row of cells within the cochlea is striking and suggests precise regulation. In *Drosophila*, Tartan and Capricious are regulated by Apterous (Lhx2; Milán and Cohen, 2003; Milán et al., 2005). However, neither Lhx2, nor the related Lhx9, have been reported to be expressed in the developing cochlea. In another context, Lrrn1 expression was shown to be controlled through binding of Mycn,

a bHLH transcription factor, to two E-box motifs in its promoter and first intron (Hossain et al., 2008), so Lrrn1 may be directly regulated by Atoh1 or other bHLHs. Atoh1 expression is not restricted to the medial boundary, though, so additional regulatory mechanisms would be required. Another possible regulatory mechanism for Lrrn1 expression is through the BMP4 gradient thought to specify the cochlear medial-lateral axis. A direct response requiring precise interpretation of the BMP4 gradient seems unlikely, suggesting instead that Lrrn1 expression is regulated through establishment of the medial-lateral cochlear axis. Finally, as noted by Basch et al. (2016), differentiation of the OC requires inductive signals from mesenchymal cells located on the opposite side of the cochlear basilar membrane (Montcouquiol and Kelley, 2003; Doetzlhofer et al., 2004). These yet unidentified inductive signals could also play a role in regulation of Lrrn1 expression.

In summary, the data presented here demonstrate that the leucine-rich repeat protein Lrrn1 is expressed at the medial boundary of the OC beginning around E14. Deletion of *Lrrn1* leads to defects in maintenance of this prosensory/nonsensory boundary resulting in ectopic IHCs and surrounding supporting cells. The effects of Lrrn1 are mediated through enhancing Notch signaling across this boundary, as the effects of mild inhibition of Notch signaling are enhanced in a *Lrrn1* mutant background and medial expression of the Notch target gene *Hes1* is downregulated in *Lrrn1* mutants. While the factors that limit expression of Lrrn1 to the medial edge of the OC are unknown, the precise nature of this expression pattern suggests that cellular patterning and axial specification within the cochlear duct have already occurred by E14. Finally, the precise expression of *Lrrn1* and *Lfng* along this boundary strongly suggests the existence of a process of cellular resolution that extends beyond a single morphogen gradient. Subsequent studies examining the factors the regulate *Lrrn1* expression in the cochlea could provide valuable insights regarding axial specification and cell fate determination.

References

Andreae LC, Peukert D, Lumsden A, Gilthorpe JD (2007) Analysis of Lrrn1 expression and its relationship to neuromeric boundaries during chick neural development. Neural Dev 2:22.

Atkinson PJ, Huarcaya Najarro E, Sayyid ZN, Cheng AG (2015) Sensory hair cell development and regeneration: similarities and differences. Development 142:1561–1571.

Basch ML, Brown RM 2nd, Jen HI, Semerci F, Depreux F, Edlund RK, Zhang H, Norton CR, Gridley T, Cole SE, Doetzlhofer A, Maletic-Savatic M, Segil N, Groves AK (2016) Fine-tuning of Notch signaling sets the boundary of the organ of Corti and establishes sensory cell fates. Elife 5: e19921.

Bier E, De Robertis EM (2015) Embryo Development. BMP gradients: a paradigm for morphogen-mediated developmental patterning. Science 348: aaa5838.

Blair SS (2001) Cell lineage: compartments and Capricious. Curr Biol 11: R1017–R1021.

Brooker R, Hozumi K, Lewis J (2006) Notch ligands with contrasting functions: Jagged1 and Delta1 in the mouse inner ear. Development 133:1277–1286.

Brückner K, Perez L, Clausen H, Cohen S (2000) Glycosyltransferase activity of Fringe modulates Notch-Delta interactions. Nature 406:411–415.

Chacon-Heszele MF, Ren D, Reynolds AB, Chi F, Chen P (2012) Regulation of cochlear convergent extension by the vertebrate planar cell polarity pathway is dependent on p120-catenin. Development 139:968–978.

Chen P, Segil N (1999) p27(Kip1) links cell proliferation to morphogenesis in the developing organ of Corti. Development 126:1581–1590.

Cohen R, Amir-Zilberstein L, Hersch M, Woland S, Loza O, Taiber S, Matsuzaki F, Bergmann S, Avraham KB, Sprinzak D (2020) Mechanical forces drive ordered patterning of hair cells in the mammalian inner ear. Nat Commun 11:5137.

de Vries WN, Binns LT, Fancher KS, Dean J, Moore R, Kemler R, Knowles BB (2000) Expression of Cre recombinase in mouse oocytes: a means to study maternal effect genes. Genesis 26:110–112.

Doetzlhofer A, White PM, Johnson JE, Segil N, Groves AK (2004) In vitro growth and differentiation of mammalian sensory hair cell progenitors: a requirement for EGF and periotic mesenchyme. Dev Biol 272:432–447.

Driver EC, Kelley MW (2010) Transfection of mouse cochlear explants by electroporation. Curr Protoc Neurosc Chapter 4:Unit 4.34.1–10.

Driver EC, Kelley MW (2020) Development of the cochlea. Development 147:dev162263.

Driver EC, Northrop A, Kelley MW (2017) Cell migration, intercalation and growth regulate mammalian cochlear extension. Development 144:3766–3776.

Ellis K, Driver EC, Okano T, Lemons A, Kelley MW (2019) GSK3 regulates hair cell fate in the developing mammalian cochlea. Dev Biol 453:191–205.

Groves AK, Fekete DM (2012) Shaping sound in space: the regulation of inner ear patterning. Development 139:245–257.

Hartman BH, Reh TA, Bermingham-McDonogh O (2010) Notch signaling specifies prosensory domains via lateral induction in the developing mammalian inner ear. Proc Natl Acad Sci U S A 107:15792–15797.

Hossain MS, Ozaki T, Wang H, Nakagawa A, Takenobu H, Ohira M, Kamijo T, Nakagawara A (2008) N-MYC promotes cell proliferation through a direct transactivation of neuronal leucine-rich repeat protein-1 (NLRR1) gene in neuroblastoma. Oncogene 27:6075–6082.

Irizarry J, Stathopoulos A (2021) Dynamic patterning by morphogens illuminated by cis-regulatory studies. Development 148:dev196113.

Jacques BE, Puligilla C, Weichert RM, Ferrer-Vaquer A, Hadjantonakis A-K, Kelley MW, Dabdoub A (2012) A dual function for canonical Wnt/β-catenin signaling in the developing mammalian cochlea. Development 139:4395–4404.

Kersigo J, Pan N, Lederman JD, Chatterjee S, Abel T, Pavlinkova G, Silos-Santiago I, Fritzsch B (2018) A RNAscope whole mount approach that can be combined with immunofluorescence to quantify differential distribution of mRNA. Cell Tissue Res 374:251–262.

Kiernan AE, Ahituv N, Fuchs H, Balling R, Avraham KB, Steel KP, Hrabé de Angelis M (2001) The Notch ligand Jagged1 is required for inner ear sensory development. Proc Natl Acad Sci U S A 98:3873–3878.

Kiernan AE, Cordes R, Kopan R, Gossler A, Gridley T (2005) The Notch ligands DLL1 and JAG2 act synergistically to regulate hair cell development in the mammalian inner ear. Development 132:4353–4362.

Kiernan AE, Xu J, Gridley T (2006) The Notch ligand JAG1 is required for sensory progenitor development in the mammalian inner ear. PLoS Genet 2:e4.

Kolla L, Kelly MC, Mann ZF, Anaya-Rocha A, Ellis K, Lemons A, Palermo AT, So KS, May JC, Orvis J, Burns JC, Hertzano R, Driver EC, Kelley MW (2020) Characterization of the development of the cochlear epithelium at the single cell level. Nat Commun 11:2389.

Lander AD (2007) Morpheus unbound: reimagining the morphogen gradient. Cell 128:245–256.

Lanford PJ, Lan Y, Jiang R, Lindsell C, Weinmaster G, Gridley T, Kelley MW (1999) Notch signalling pathway mediates hair cell development in mammalian cochlea. Nat Genet 21:289–292.

Madisen L, Zwingman TA, Sunkin SM, Oh SW, Zariwala HA, Gu H, Ng LL, Palmiter RD, Hawrylycz MJ, Jones AR, Lein ES, Zeng H (2010) A robust and high-throughput Cre reporting and characterization system for the whole mouse brain. Nat Neurosci 13:133–140.

Mao Y, Kerr M, Freeman M (2008) Modulation of *Drosophila* retinal epithelial integrity by the adhesion proteins Capricious and Tartan. PLoS One 3:e1827.

McKenzie E, Krupin A, Kelley MW (2004) Cellular growth and rearrangement during the development of the mammalian organ of Corti. Dev Dyn 229:802–812.

Milán M, Cohen SM (2003) A re-evaluation of the contributions of Apterous and Notch to the dorsoventral lineage restriction boundary in the *Drosophila* wing. Development 130:553–562.

Milán M, Weihe U, Pérez L, Cohen SM (2001) The LRR proteins Capricious and Tartan mediate cell interactions during DV boundary formation in the *Drosophila* wing. Cell 106:785–794.

Milán M, Pérez L, Cohen SM (2005) Boundary formation in the *Drosophila* wing: functional dissection of Capricious and Tartan. Dev Dyn 233:804–810.

Mizutari K, Fujioka M, Hosoya M, Bramhall N, Okano HJ, Okano H, Edge AS (2013) Notch inhibition induces cochlear hair cell regeneration and recovery of hearing after acoustic trauma. Neuron 77:58–69.

Moloney DJ, Panin VM, Johnston SH, Chen J, Shao L, Wilson R, Wang Y, Stanley P, Irvine KD, Haltiwanger RS, Vogt TF (2000) Fringe is a glycosyltransferase that modifies Notch. Nature 406:369–375.

Montcouquiol M, Kelley MW (2003) Planar and vertical signals control cellular differentiation and patterning in the mammalian cochlea. J Neurosci 23:9469–9478.

Mueller KL, Jacques BE, Kelley MW (2002) Fibroblast growth factor signaling regulates pillar cell development in the organ of Corti. J Neurosci 22:9368–9377.

Munnamalai V, Fekete DM (2016) Notch-Wnt-Bmp crosstalk regulates radial patterning in the mouse cochlea in a spatiotemporal manner. Development 143:4003–4015.

Ohyama T, Basch ML, Mishina Y, Lyons KM, Segil N, Groves AK (2010) BMP signaling is necessary for patterning the sensory and nonsensory regions of the developing mammalian cochlea. J Neurosci 30:15044–15051.

Orvis J, et al. (2021) gEAR: gene expression analysis resource portal for community-driven, multi-OMIC data exploration. Nat Methods 18:843–844.

Pan W, Jin Y, Stanger B, Kiernan AE (2010) Notch signaling is required for the generation of hair cells and supporting cells in the mammalian inner ear. Proc Natl Acad Sci U S A 107:15798–15803.

Pan W, Jin Y, Chen J, Rottier RJ, Steel KP, Kiernan AE (2013) Ectopic expression of activated notch or SOX2 reveals similar and unique roles in the development of the sensory cell progenitors in the mammalian inner ear. J Neurosci 33:16146–16157.

Panin VM, Papayannopoulos V, Wilson R, Irvine KD (1997) Fringe modulates Notch-ligand interactions. Nature 387:908–912.

Prajapati-DiNubila M, Benito-Gonzalez A, Golden EJ, Zhang S, Doetzlhofer A (2019) A counter gradient of Activin A and follistatin instructs the timing of hair cell differentiation in the murine cochlea. Elife 8:e47613.

Radtke F, Wilson A, Stark G, Bauer M, van Meerwijk J, MacDonald HR, Aguet M (1999) Deficient T cell fate specification in mice with an induced inactivation of Notch1. Immunity 10:547–58.

Rubel EW (1978) Ontogeny of structure and function in the vertebrate auditory system. In: Handbook of sensory physiology (Jacobson M, ed), pp 135–237. New York: Springer.

Taguchi A, Wanaka A, Mori T, Matsumoto K, Imai Y, Tagaki T, Tohyama M (1996) Molecular cloning of novel leucine-rich repeat proteins and their expression in the developing mouse nervous system. Brain Res Mol Brain Res 35:31–40.

Tateya T, Imayoshi I, Tateya I, Ito J, Kageyama R (2011) Cooperative functions of Hes/Hey genes in auditory hair cell and supporting cell development. Dev Biol 352:329–340.

Tossell K, Andreae LC, Cudmore C, Lang E, Muthukrishnan U, Lumsden A, Gilthorpe JD, Irving C (2011) Lrrn1 is required for formation of the midbrain-hindbrain boundary and organiser through regulation of affinity differences between midbrain and hindbrain cells in chick. Dev Biol 352:341–352.

Urness LD, Wang X, Shibata S, Ohyama T, Mansour SL (2015) Fgf10 is required for specification of non-sensory regions of the cochlear epithelium. Dev Biol 400:59–71.

Wang J, Dahmann C (2020) Establishing compartment boundaries in *Drosophila* wing imaginal discs: an interplay between selector genes, signaling pathways and cell mechanics. Semin Cell Dev Biol 107:161–169.

Wu DK, Kelley MW (2012) Molecular mechanisms of inner ear development. Cold Spring Harb Perspect Biol 4:a008409.

Wurst W, Bally-Cuif L (2001) Neural plate patterning: upstream and downstream of the isthmic organizer. Nat Rev Neurosci 2:99–108.

Xiang M, Gao WQ, Hasson T, Shin JJ (1998) Requirement for Brn-3c in maturation and survival, but not in fate determination of inner ear hair cells. Development 125:3935–3946.

Yamamoto N, Okano T, Ma X, Adelstein RS, Kelley MW (2009) Myosin II regulates extension, growth and patterning in the mammalian cochlear duct. Development 136:1977–1986.

Zhang N, Martin GV, Kelley MW, Gridley T (2000) A mutation in the Lunatic fringe gene suppresses the effects of a Jagged2 mutation on inner hair cell development in the cochlea. Curr Biol 10:659–662.

Zhang X, Lee SJ, Young MF, Wang MM (2015) The small leucine-rich proteoglycan BGN accumulates in CADASIL and binds to NOTCH3. Transl Stroke Res 6:148–155.

Zhang Y, Liu Q, Yang S, Liao Q (2021) Knockdown of LRRN1 inhibits malignant phenotypes through the regulation of HIF-1α/Notch pathway in pancreatic ductal adenocarcinoma. Mol Ther Oncolytics 23:51–64.

Zine A, Aubert A, Qiu J, Therianos S, Guillemot F, Kageyama R, de Ribaupierre F (2001) Hes1 and Hes5 activities are required for the normal development of the hair cells in the mammalian inner ear. J Neurosci 21:4712–4720.